MASTER OF PHILOSOPHY

Investigation of the Effect of Superhydrophobic Coatings on the Performance of Heat Exchangers

Li, Yanran

Award date:
2017

Awarding institution:
Queen's University Belfast

Investigation of the Effect of Superhydrophobic Coatings on the Performance of Heat Exchangers

Yanran Li

Principal Supervisor: Prof. Steven E.J. Bell

Second Supervisor: Dr. Chirangano Mangwandi

A Thesis Submitted to

the School of Chemistry and Chemical Engineering

The Queen's University of Belfast

For the Degree of Master of Philosophy

2017

Abstract

The main aim of this project was to investigate the effect of superhydrophobic coatings on the performance of aluminium louvered fin heat exchangers. A method was developed to prepare superhydrophobic coatings on the exchangers by applying layer of metallic zinc and then reacting the zinc-coated exchanger with silver to electrolessly deposit a microscopically rough silver layer. This was then treated with a polyfluorothiol compound to create a self-assembled monolayer with low surface energy, giving a superhydrophobic coating, or an alcohol terminated thiol to give a superhydrophillic coating. Initial tests of louvered-fin heat exchangers with both these coatings showed they retained significant amounts of condensed water when they were used to cool air to below the dew point. This condensed water affected both the stability of the coatings and the resistance to air flow through the heat exchangers. An alternative approach to preparing superhydrophobic coatings was then also adopted in which superhydrophobic copper powder was fixed onto the heat exchanger using a thin adhesive layer. Dynamic dip tests were conducted with the coated and uncoated heat exchangers suspended vertically and horizontally. With the normal vertical mounting the superhydrophobic zinc/silver coated heat exchanger surprisingly retained more water than the untreated heat exchanger and much more water than the hydrophilic heat exchanger. This was due to the coating interfering with the drainage of water through the narrow channels which are designed to allow water to escape in uncoated heat exchangers. Conversely, with the heat exchangers suspended horizontally, the advantage of the superhydrophobic coating was apparent since the system retained significantly less water than the uncoated control.

However, under normal operating conditions the superhydrophobic coating did not give the same improvement due to flooding of the textured surface under high water condensation rates. The thermal performance of the coated and uncoated heat exchangers was measured with a simple test apparatus which was built for this purpose and allowed control of the input air temperature, humidity and velocity. This system also allowed measurement of the inlet and outlet air temperature and relative humidity as well as inlet and outlet water temperature, thus enabling overall heat transfer coefficient to be calculated. It was found that the overall heat transfer coefficient generally increased with inlet air velocity for all heat exchangers. However, comparison of the coated and uncoated heat exchangers at similar input velocities showed that the calculated the heat transfer coefficients of all the exchangers were similar. There may have been small improvements due to dropwise condensation on the surfaces but this was more than counterbalanced by the increased pressure drop observed for the coated heat exchangers due to retained water. This means that the overall performance of even the horizontally mounted superhydrophobic coated systems, which showed very favourable water shedding properties under bulk water testing, was not improved in water condensation experiments. This main source of this effect is the flooding of the superhydrophobic surfaces at high condensation rates, an effect which will need to be addressed if the potential advantages of superhydrophobic surfaces are to be realised in real heat exchange systems.

Acknowledgement

First of all, I would like to express my deepest gratitude to my principal supervisor, Professor Steven Bell, who always gave me valuable guidance and full support throughout the research. He always keeps kindness and patience to help me solving problems whenever I have questions in experiments or writing. And also express my thanks to my second supervisor, Dr.Chirangano Mangwandi, who showed interest in how I was getting on and also gave me instructions.

I would like to give thanks to John McCracken, a PhD student in our group, who always helped me to do experiments and sorted lots of problems. Besides, thank you for kindly giving me lots of papers related to my research.

I would also like to thank other members in our groups, thank you for your help in studying or in life during this whole year.

My family, especially my parents, showed fully support of my life and study, financially and emotionally. Without you, I could not have the opportunity to do research abroad. Thank you for your encouragement.

I would like to express special thanks to my housemates, who were always be there for me and made me feel at home. And also to thank my friends in Belfast, thank you for your warm company. My friends in China and other places, time and distance could not be barriers to our friendships. Thank you all for supporting me all the time.

Contents

Chapter 1 Introduction

Chapter 1 Introduction

Background

The investigation of superhydrophobic surfaces has expended rapidly since the first report by Barthlott and Neinhuis[1] of the extreme hydrophobicity shown by various plant leaves. The topic bridges areas of physics, chemistry, biology and materials science since it involves observation of natural phenomena, coupled with theoretical studies and attempts to prepare artificial superhydrophobic materials. The area has attracted considerable interest because of the potential practical benefits that may result from superhydrophobicity including self-cleaning, drag-reduction, anti-fogging, and anti-icing. The area of interest within this thesis is that of improving energy efficiency through coating heat exchangers. Energy efficiency is one of the most important topics for sustainable development. Heating, ventilation and AC (HVAC) systems are an important contributor to overall energy consumption both in industries and in households. According to a recent EC research centre's report[2], HVAC systems accounted for approximately 11 % of the total electricity consumed in Europe in 2007. Since heat exchangers are one of the most important parts in HVAC systems, any reduction of in their energy use could give very large total energy savings.

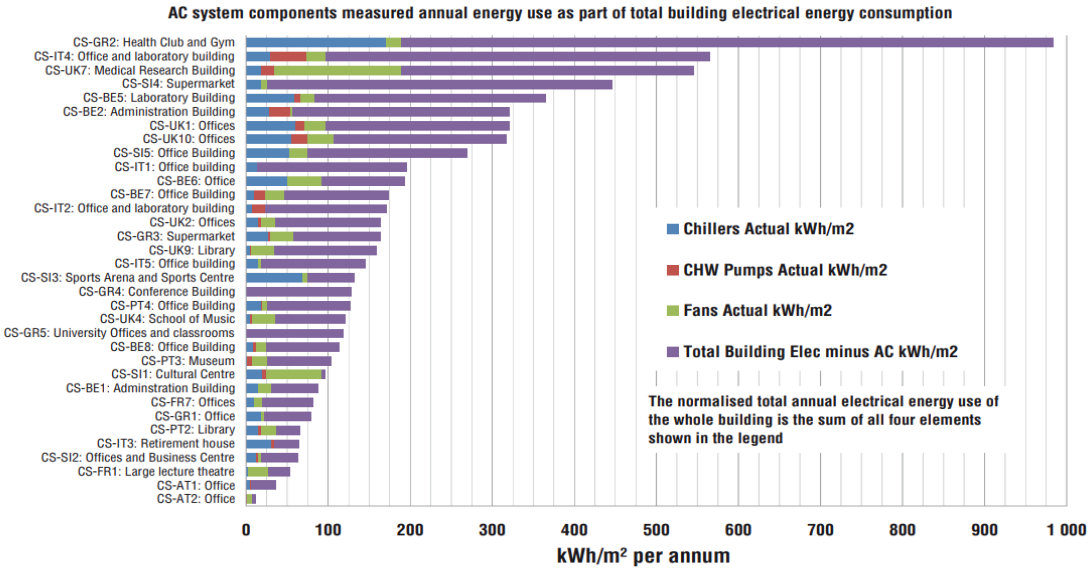

Figure 1.1 Overall annual energy use and total energy use in 33 HARMONAC buildings[3].

In an earlier unpublished preliminary study carried out at QUB, J. McCracken found that an evaporator coated so that it had a superhydrophobic surface used much less energy than an uncoated evaporator to achieve the same cooling. The purpose of the current work was to build on this earlier small study with a more comprehensive investigation into the effect of superhydrophobic coatings on commercially relevant aluminium tube and fin heat exchangers.

1.1 Definitions

Hydrophobicity describes the preference of a liquid drop to be in contact with solid surface. The contact angle and sliding angle are the important measurable characteristics to describe hydrophobicity, which indicates the degree of wetting when a solid and liquid interact.

1.1.1 Contact Angle

The contact angle is defined as the angle between the tangent to the liquid-liquid interface and the tangent to the solid interface at the contact line between the three phases (shown in Figure 1.2). If a surface has a large contact angle it means that the real contact area between the adhering droplet and the surface is very small compared to surfaces with a low contact angle.

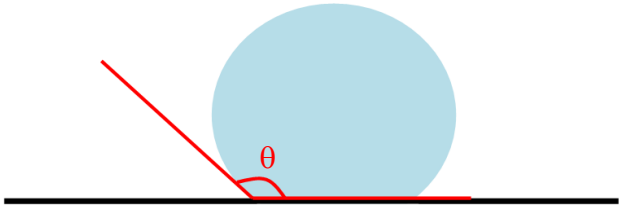

Figure 1.2 The contact angle (θ) of a water droplet on a solid surface.

The first equation to describe contact angle was proposed by Thomas Young [4] who related it to the surface tensions involved.

$$\cos\theta = \frac{\gamma_{SV} - \gamma_{SL}}{\gamma_{LV}} \qquad (1.1)$$

Where θ is the measured contact angle, γ_{SV} is the solid-vapour surface tension, γ_{SL} is the solid-liquid surface tension and γ_{LV} is the liquid surface tension. This equation is based on an ideal surface, i.e. the surface is chemically homogenous and topographically smooth.

Later, Robert Wenzel showed that surface wettability could be enhanced by increasing surface roughness, which can be achieved by altering the chemistry of the surface.[5] He corrected Young's contact angle equation by adding a roughness factor.

$$\cos\theta_W = r\cos\theta_Y \quad (1.2)$$

Where θ_W is the measured contact angle on a rough substrate, r is the roughness factor and θ_Y is the Young's contact angle. The roughness factor is a measure of how surface roughness affects a homogenous surface and is defined as the ratio between the actual and projected solid surface area (r=1 for a smooth surface and r>1 for a rough one).

The Wenzel regime is described as the state where the liquid fully penetrates the gap between roughness features causing the complete wetting of the surface.

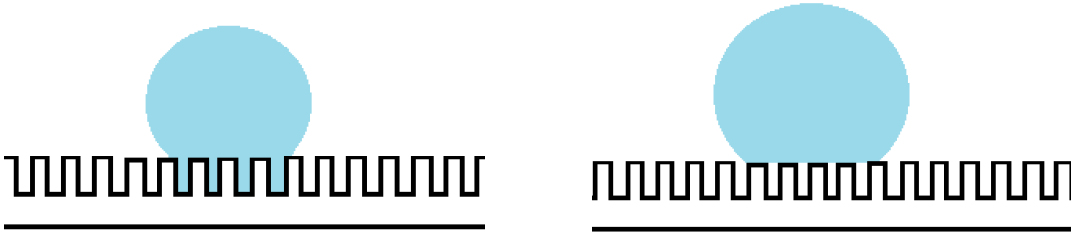

Figure1.3 (a) Wenzel model (b) Cassie-Baxter model

In contrast to the Wenzel model, the Cassie-Baxter regime is a situation in which air is trapped in the rough surface features, causing the water droplet to stay on top of a layer of air.[6] The regime is associated with superhydrophobic surfaces which have large roughness in combination with very low surface energy. The high interfacial energy between liquid and air leads to a higher contact angle on the rough than the smooth surface.

$$\cos\theta_{C-B} = f_1\cos\theta_1 + f_2\cos\theta_2 \quad (1.3)$$

Where $\theta_{C\text{-}B}$ is the measured contact angle, f_1 is the fraction of constituent one, θ_1 is the Young's contact angle of constituent one, f_2 is the fraction of

constituent two and θ_2 is the Young's contact angle of constituent two. If one of the constituents is air, the equation can be simplified as shown.

$$\cos\theta_{C-B} = -1 + f_1(\cos\theta_1 + 1) \tag{1.4}$$

1.1.2 Contact Angle Hysteresis

The contact angles formed by expanding and contracting the liquid are referred to as the advancing contact angle, θ_a and receding contact angle, θ_r, respectively. These angles define a range, with the advancing angles approaching a maximum value, and the receding angles approaching a minimum value. The advancing contact angle can be measured by inflating a liquid drop on a substrate surface, while the receding contact angle θ_r is measured for a shrinking liquid drop on the surface.[7] The difference between the advancing angle and receding angle is called the hysteresis (H):

$$H = \theta_a - \theta_r \tag{1.5}$$

The size of the hysteresis determines the extent of adhesion of a liquid droplet to a surface.

1.1.3 Sliding Angle

When analyzing the hydrophobicity of a material, the measurement of contact angle is not sufficient. The sliding angle, which is the angle at which a drop of known mass begins to move on a surface, is also considered as an important characteristic of the surface.

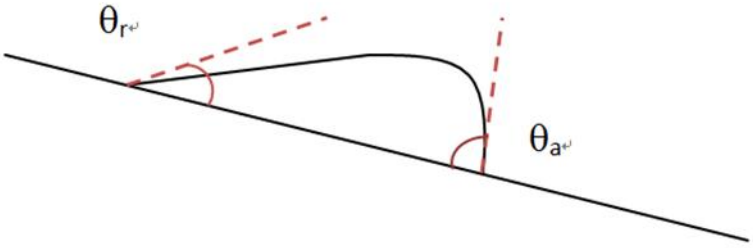

Figure 1.4 Diagram of the advancing and receding angles of a droplet on an inclined surface.

The sliding or tilt angle is determined by values of the advancing and receding angles, as shown below.

$$\sin\alpha \approx \frac{\gamma_{LV}\,2r}{mg}\left(\cos\theta_r - \cos\theta_a\right) \tag{1.6}$$

Where α is the sliding/tilt angle, γ_{LV} is the surface tension of the test liquid, r is the drop radius, m is the drop mass, g is the acceleration due to gravity. Since this equation contains the contact angle hysteresis, the smaller the hysteresis the smaller the sliding/tilt angle will be, therefore it is possible to have a surface where drops show low contact angles but still have very low sliding angles. Conversely, it is also possible to have a surface that demonstrates a superhydrophobic contact angle but a very large hysteresis, resulting in drops being stuck even when the surface is tilted upside down. The sliding angle therefore indicates whether the surface is slippery or sticky. When the sliding angle is low, the liquid has low adhesion to the surface.

1.1.4 Superhydrophobicity

The wettability of a surface can be defined through the contact angle. From

the Young's equation, if $\gamma_{SV}<\gamma_{LV,}$ the contact angle is less than 90° and the surface is defined as hydrophilic. If $\gamma_{SV}>\gamma_{LV,}$ the contact angle is greater than 90° and the surface is classed as hydrophobic. In general, a hydrophobic surface can be further defined as 'superhydrophobic' if the contact angle is greater than 150° [8]. Some researchers have suggested that the contact angle is not enough and to be superhydrophobic the surface contact angle should be more than 150° and the contact angle hysteresis less than 10°.[9] There are many plants and animals in nature that have the ability to repel water. The first reported superhydrophobic object was the lotus leaf, which shows both high water repellency and self-cleaning ability. Barthlott and Neinhuis[1] measured the contact angle of lotus leaves at 162° which was the highest among the compared species. They were the first to report that the lotus leaves' very high contact angle due to a combination of a double roughness structure and a low surface energy wax coating. Besides lotus leaves, plants were found to have water repellency. For example, rose petals were found to exhibit superhydrophobicity but with high water adhesion.[10] Superhydrophobicity also exits in animals.[11-15] For example, some insects such as water spiders have the ability to walk on the water surface due to the hairs on their legs which could trap a high volume of air to provide resistance to liquid impregnation.[14] Many insert wings also were found to have the highly ordered nanostructures which provide high hydrophobicity.[13, 16]

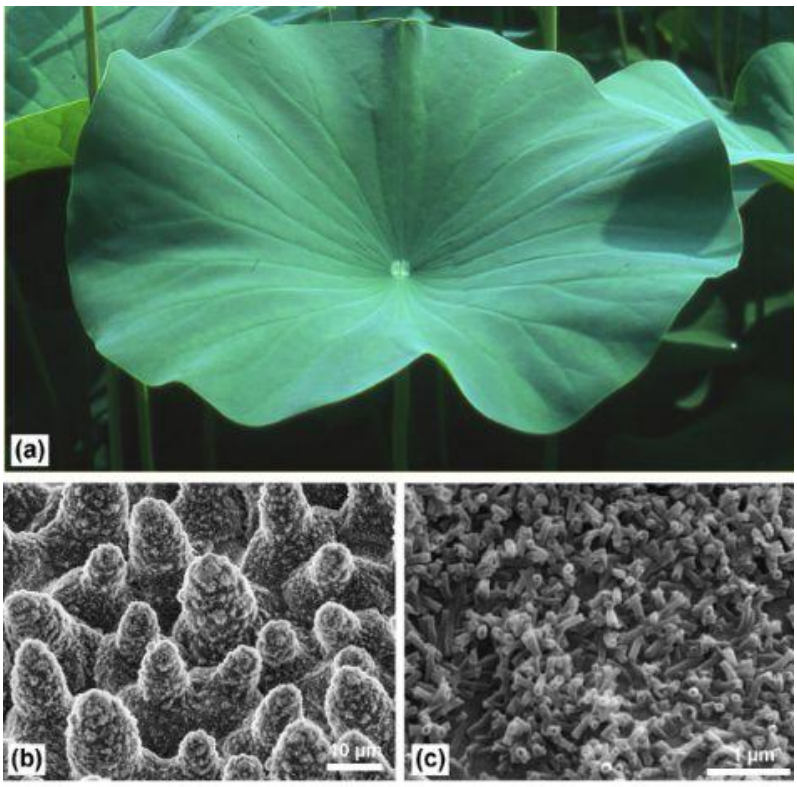

Figure 1.5 (a) Lotus leaves (b) Scanning electron microscopy (SEM) image of the lotus leaf side prepared by 'glycerol substitution' (c) Wax tubules on the upper leaf side.[17]

1.1.5 Applications of Superhydrophobic Surfaces

The wide range of potential applications of superhydrophobic surface has drawn much interest in recent years. For example, resistance to metal corrosion can be achieved by a layer of superhydrophobic coating on the surface.[18, 19] Liu *et al.*[20] coated a superhydrophobic film on zinc which could protect the zinc interface in a NaCl solution for up to one month. Inspired by the lotus leaf, self-cleaning artificial material is also a potential application. The high contact angle and low roll-off angle of superhydrophobic surfaces allow rolling droplets to clean the surface by carrying away the dust particles which can be used in various applications such as windows and solar panels.[21] Drag-reduction in pipeline water transportation is another potential

application. If the system is in a Cassie-Baxter state, the contact between water and solid surface is reduced by a layer of air which may also reduce the friction felt by the water flowing through the pipe.[22, 23] Another interesting application of superhydrophobic surfaces is in oil-water separation as reported by few researchers.[24, 25] A porous material with a high water contact angle and with an extremely low or 0° oil contact angle can allow oil to flow through the surface but prevent water flow.

1.2 Methods to Achieve Superhydrophobicity

Superhydrophobicity can be achieved either by increasing the roughness of the surface or lowering the surface energy, normally referred to as the chemical method.

1.2.1 Electrodeposition

Electrodeposition is a widely-used metal deposition technology used to coat a thin layer of metal on top of another metal to achieve the desired electrical and corrosion resistance, reduce friction, improve heat tolerance or for decoration.[26] In electrochemical deposition, a thin metal layer is deposited onto the surface of specimen from a solution containing ions or charged micro/nanoparticles.

The morphology of the deposited surface varies according to the current density used during electrodeposition. Xi[27] electroplating the copper in an aqueous solution composed of $CuSO_4$ and H_2SO_4, the treated surface of the copper showed the similar structure as lotus leaf. The contact angle and sliding angle were 153.4°and 7°, respectively. Min Ho Kwa[28] used a

pulsed laser system for micro-structuringfound and then electrodeposit the copper in an aqueous solution of 0.5 M copper sulfate pentahydrate and 0.5 M sulfuric acid. They found that in oxidation of copper over a large range of the current densities, higher current density resulted in a rougher surface. Pijakova *et al.*[29] coated a stainless steel plates by one-step electrodeposition. The electrolytes is 0.045 M perfluorooctanoic acid in deionized water, reaching the contact angle of 159° for deionized water, 153° for olive oil.

All deposition growth methods require careful control of voltage, concentration, temperature and treatment times to form a coating with the desired structure.

1.2.2 Spray Coated Surfaces

Spraying chemicals directly on the substrate to obtain artificial superhydrophobic surface is a fast and low-cost method. Compared with other methods, spraying has no restrictions on substrate shape and size and can be implemented with only a spray gun and an air pump.[30] Wu[31] created a superhydrophobic coating by spray-coating metal alkycarboxylates, $Cu[CH_3(CH_2)_{10}COO]_2$ directly onto substrates. A contact angle of 158°±2° and a sliding angle of 5° were achieved using the proper concentrations of regents. Ogihara *et al.*[32] made superhydrophobic paper by spraying ethanol suspensions of SiO_2 nanoparticles which reached a contact angle of 153° after coating. Another advantage of this method is the coating can be reapplied if damaged.

1.2.3 Templating

The templating method is widely used in surface fabrication of micro/nano structures. It is a cost-effective and accurate controllable method to fabricate a surface. Generally, the templating process includes preparing a featured template master, then modelling the replica and finally removing the template.[33] A surface treated by lithography can be further processed using plasma etching to achieve complex roughness.

Cho *et al*[34] used an anodic aluminium oxide membrane as a replication template to create the hairy hard poly(dimethysiloxane) layer on substrate. The surface showed good superhydrophobicity with a contact angle of 150°.

1.2.4 Sol-gel Methods

Sol-gel methods have been widely used in preparing superhydrophobic surface because of the advantages of low temperature and high homogeneity of final products.[35]

Fang *et al.*[25] prepared a superhydrophobic film on a glass by using aluminium-*sec*-butoxide solution. The film was immersed in boiling water and reheated before modifying with fluoroalkylsilane. The contact angle was 168.3°. Shi *et al* [36] formed a superhydrophobic coating by using hydrolysis of a chelate compound of aluminium isopropoxide and ethyl acetoactate. Stearic acid/hexane solution was used for surface modification. The contact angle achieved was 168 ° after modification. Ma et al.[37] reported a non-sticky superhydrophobic surface which has high thermal stability and mechanical durability creating by a simple sol–gel process and a surface hydrophobicing step. This method is not restricted by the substrates which can be applied on glass, metals and polymer surface with little or no

pretreatment.[38] In addition it requires a relatively ambient treatment temperature and a short application time.

1.2.5 Chemical Vapour Deposition (CVD)

Chemical vapour deposition is a method to deposit a solid product onto a substrate by means of a gas phase or surface reaction. The precursors are vaporized and then chemical reactions take place on the cold substrate. There are several ways to activate the reactant: heating, electromagnetic radiation and plasma activation.

Lau *et al.* [39] created a superhydrophobic polytetrafluoroethylene coating on the surface of the carbon nanotubes through a hot filament chemical vapour deposition process. Razaei *et al.*[40] prepared a superhydrophobic surface by one-step chemical vapour deposition using tertraethoxysilane, vinyltrimethoxysilane as the surface modifying molecules. The method combined surface roughness and low surface energy to create superhydrophobic layer of silica-coated surface with contact angle over 170°.

1.2.6 Chemical Etching

Compared with other methods, chemical etching is a fast, simple and easily controlled way to form superhydrophobic surface. Qian and Shen[41] prepared superhydrophobic surfaces on aluminium, copper and zinc by etching with hydrochloric acid and hydrophobizing with fluoroalkysilane at room temperature. The surfaces after treatment showed good superhydrophobicity with contact angle more than 150° and sliding angle less than 10°. Lee and Choi[42] combined chemical etching and spin-coating

processes. They deposited Cu on the silicon surface then immersed the Cu-coated plate in a mixture of HF/H_2O_2 solution to etch the silicon substrate to create a rough surface. The copper was then removed by strong nitric acid followed by coating with a layer of Teflon. The contact angle reached nearly 180°. Wang *et al.*[43] etched the polished aluminium by immersing in HNO_3/H_2O_2 mixed solutions. The substrate was then immersed in a solution of stearic acid and N,N'-dicyclohexylcarbodiimide (DCCD) in n-hexane (5 mmol/L) for 24 h. The contact angle of the surface was 156° after modified.

1.2.7 Electroless Deposition

Electroless deposition is a good technique compared to electrodeposition method to prepare the rough surface required for superhydrophobicity since it does not require special equipment and it allows easy process control. Larmour and Bell[44] developed a method for preparing superhydrophobic surfaces based on an electroless deposition process with chemical modification using fluorinated thiol. Zinc or copper sheets were cleaned with acetone and absolute ethanol and immersed in $AgNO_3$ to coat them with electrolessly deposited silver. The coated metal was then dipped into 3,3,4,4,5,5,6,6,7,7,8,8,9,9,10,10,10-heptadecafluoro-1-decanethiol (HDFT) in dichloromethane for five minutes and rinsed. Although this method is very quick and simple, it produced surfaces with a tilt-angle of 0.64°±0.04° and a high contact angle of 173°±1°. When the coated metal immersed in water, a 'silver mirror' was observed at a titled angle showing the air layer was approached between the bulk water and surface which proved the Cassie-Baxter state was achieved.

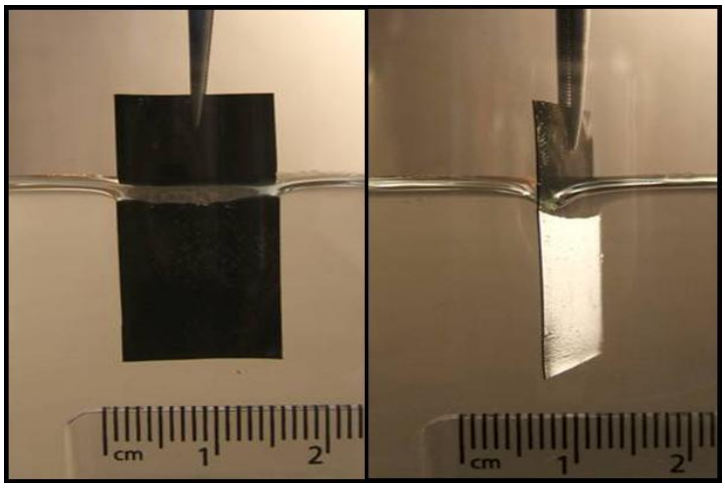

Figure 1.6 Demonstration of the highly reflective 'silver mirror' observed when an electrolessly deposited superhydrophobic surface was viewed at a glancing angle under water.[44]

Other workers have used similar approaches. Xu *et al.*[45] prepared a superhydrophobic copper plate modified with n-octadecanethiol after electroless deposition. The contact angle of the surface was 169±2° and sliding angle was 2°. Ogihara *et al.*[46] deposited Ni on copper plates for more than 60 min before thermal treatment followed by trimethylsiloxysilicate (TMSS) deposition. The contact angle of the treated copper plate was around 150°. Tian[47] fabricated a nickel surface by coupling electro- and electroless deposition without chemical modification, reaching a contact angle of 153.6°. Wood *et al.*[48] functionalized the surface with pulsed plasma poly(4-vinylpyridine) and then by zinc deposition for 2 hours catalyzed by palladium. The contact angle of the surface was over 150° after modification. Another electroless deposition method to achieve superhydrophobic surface with a contact angle of 165° was reported by Muench *et al.*[49] The substrates were treated using an electroless silver plating bath and then reacted for galvanic Au exchange followed by application of a self-assembled thiol monolayer (1-hexadecanethiol).

Although many methods for preparing superhydrophobic coatings by

electroless deposition have been reported, Bell's method was found to have higher performance and shorter preparation time compared with these other methods.

1.3 Heat Exchangers

Heat Exchangers are devices used to transfer heat between two or more fluids in order to cool or heat a system. Heat exchangers are widely used in heating, refrigeration, air conditioning systems, power plants, chemical plants, petrochemical plants, petroleum refineries, natural gas processing and sewage treatment. Heat exchangers can be divided into compact heat exchangers and non-compact heat exchangers.[50] Compact heat exchangers are characterized by having a large ratio of heat transfer surface to heat exchanger volume. It has been reported that compact heat exchangers are essential to energy saving and high-efficiency energy utilization.[51] Plate heat exchangers, plate-tube heat exchangers and finned-tube heat exchangers are all different types of compact heat exchanger. Finned-tube heat exchangers can be further classified by their shape i.e. wavy-fin versus and louvered-fin designs. In the current study, compact heat exchanger with louvered fins is used. Louver fin pattern is one of the most advanced of the extended fin surfaces. Compared with other compact heat exchangers, louvered fin heat exchangers show great performance on enhancing heat transfer with smaller size, weight and cost. Louvered-fin heat exchangers are commonly used to break up boundary growth and increase the air side heat transfer area. For these reasons, they are widely used for automotive applications.

The working mechanism of air conditioning system can be explained using an automobile system as an example where the evaporator is a

louvered-fin heat exchanger. There are five major components in the system (shown in Figure 1.7): these are the compressor, condenser, receiver-dryer, expansion valve and the evaporator. The compressor is the starting point of the whole air conditioner system. When the system is switched on, the compressor starts to turn and pump the refrigerant vapour under high pressure to the condenser. The vapour then is condensed to a liquid inside condenser to reduce the generation of redundant heat. A fan is installed before the condenser to draw air thorough it and cool the refrigerant. The liquid refrigerant movies to the receiver-dryer to remove any moisture that may cause ice crystals causing blockage and mechanical damage. The refrigerant then passes through a valve to the evaporator which is where the coldness is created. When the cold low-pressure refrigerant fluid enters the evaporator, it vaporizes and absorbs heat from the surroundings. The blower fan inside the passenger compartment draws air over the outside of the evaporator, cooling the air which is then circulated inside the car.

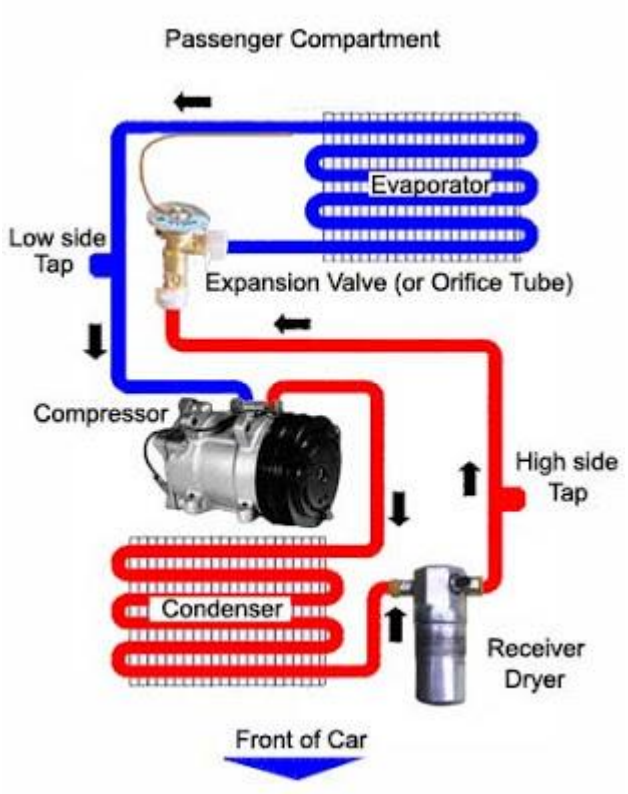

Figure 1.7 Diagram of an automobile air conditioner system.[52]

1.4 Condensation

Vapour condensation is a very common phenomenon. In cooling systems the evaporator normally operates below the dew point of the ambient air so that water vapour condenses and accumulates on the heat transfer surfaces. Condensation is retained on the surface until removed by gravity or an air flow. Increasing of retention in the air side of heat exchangers affects the heat transfer by blocking the air flow path, especially for high density fin heat exchangers. The blockage of air side of heat transfer will increase pressure drop and the water film will have a large thermal resistance. Both these effects lead to higher power consumption. The condensation inside the air side of evaporator is a potential site for growing bacteria which can have a

bad impact on the indoor air quality. The condensation also reduces the outlet humidity which may cause discomfort. The control of water retention therefore plays an important role for both energy efficiency and the quality of the cooled environment.

When moist air condenses on a surface, it can do so in dropwise mode, filmwise mode or a mixed mode. For the dropwise condensation, the liquid phase collects as individual droplets, which means the surface is not fully wetted by the condensate. In filmwise condensation, the surface is completely wetted by the condensate and so is covered by a liquid film. The water droplets generated on the surface sit without spreading out, which means that the thermal resistance caused by the water film is reduced. It has been confirmed experimentally that the heat transfer for dropwise condensation is around five to seven times larger than for filmwise condensation under the same experimental conditions.[53] This makes dropwise condensation very attractive for industrial applications. It is known that the condensation mode mainly depends on the surface wettability. Many reports[54-56] have shown that the size of the drops and the contact angle play important roles in condensation. Surfaces with high contact angle tend to enhance dropwise condensation and surfaces with low contact angle are more likely to show filmwise condensation. It has been shown that the smaller drops can transfer more heat per unit contact area.[57] The size of the departing drops can be reduced by increasing the contact angle, which in turn allows more condensation surface for nucleating drops.

Dropwise condensation was first reported by Schmidt *et al.*[58] and since that time models of dropwise condensation have been developed. Fevre and Rose[59] developed the first dropwise condensation heat transfer model. Their model includes three thermal resistances: conduction resistance,

vapour-liquid interfacial resistance and surface resistance. Wen *et al.*[60] developed an expression for calculation of dropwise condensation heat transfer by classifying the droplets into two groups: small droplets before coalescence and large droplets after coalescence. Kim and Kim[54] established a model by combining the heat transfer through a single droplet with the drop size distribution and therefore developed a mathematical model for the calculation of dropwise condensation heat transfer for superhydrophobic surface treatments. The model considered all the thermal resistance between the vapour and the condenser surface.

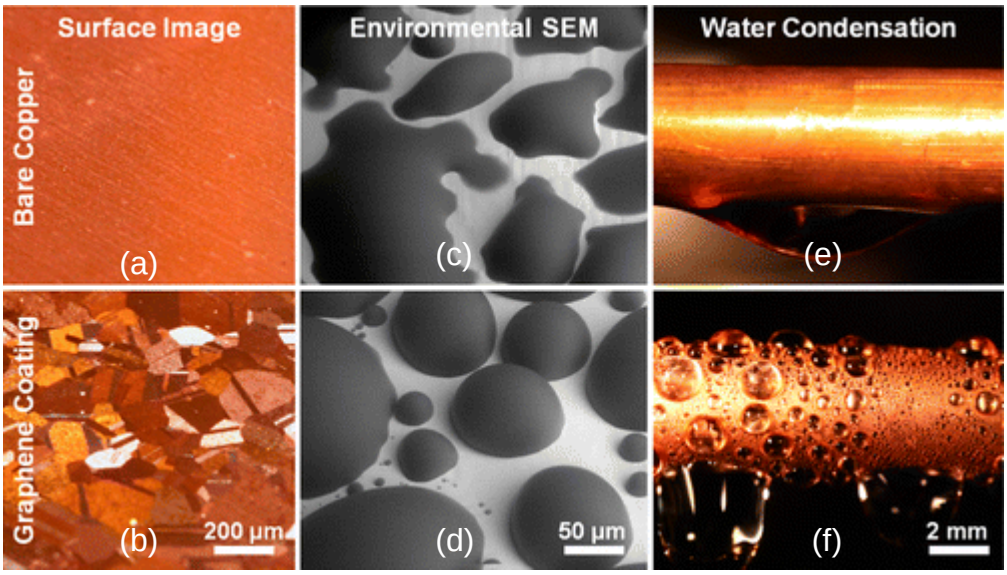

Figure 1.8 Surface images of bare copper (a) and grapheme coated copper (b). SEM images of water condensation on bare copper surface (c) and graphene coated copper (d). Photographs of pipe under filmwise condensation (e) and dropwise condensation (f).[61]

Although dropwise condensation can be achieved with surfaces with high contact angles which are still far from superhydrophobic, there have been several studies investigating condensation onto genuinely superhydrophobic materials with the objective of understanding the process and ultimately how this might be exploited in heat exchangers. The rationale

is that reduction of sliding angle and increase of contact angle of the material should in principle promote removal of the condensed water drops from the surface, which means that the residence time of the droplets on the surface is reduced and the average droplet size is also correspondingly reduced. Both of these effects would be expected to increase heat transfer.

The obvious reason for increased droplet removal is that on the superhydrophobic surface, the condensate forms as poorly adhered near spherical droplets which grow with time but are then shed due to gravity or the air flow passing over the exchanger. In addition to the conventional loss, droplets on superhydrophobic surfaces also show surprising 'jumping' behaviour where coalescence of droplets results in a significant out of plane force which causes the condensed droplet to eject from the surface. Under conditions where the droplets simply fall back onto the surface they may not be significant but under normal heat exchanger operating conditions they may well be carried away from the exchanger by the air flow. The jumping mode was first reported by Boreyko and Chen[62], they found that the condensate on the superhydrophobic can be automatically removed by droplet coalescence and jumping. The jumping velocity of droplets can be as high as 1 m/s. It was found by Yanagisawa *et al.*[63] that the jumping velocity depended on the size difference of the droplets which were coalescing and they developed a mathematical expression which accounted for the jumping velocity when differently sized droplets coalesced. Chen *et al.* [64] focused on the coalescence-induced jumping triggered by more than two droplets. It was found a majority (> 79 %) of jumping events occured upon the coalescence of multiple droplets during the 115 coalescence events viewed. It was also observed that the highest velocities occurred when two droplets coalesced rather than multidroplet coalescing. Dietz *et al.* [65] found the

droplets with diameters less than 10 μm give the most significant contribution to heat transfer and new droplets only form once large drops departed.

All this work on simple superhydrophobic surfaces suggest that superhydrophobic coatings should improve the performance of heat exchangers. The main challenge would therefore be expected to be preparing superhydrophobic coatings on actual industrially relevant heat exchangers rather than simple test materials. This means that a method for preparing superhydrophobic coatings on aluminium objects is required.

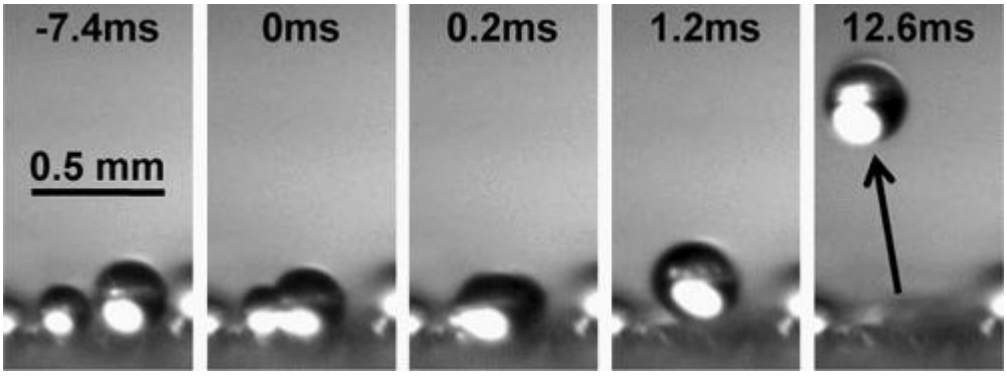

Figure 1.9 Side-view image of droplets coalesced and jumped of the surface due to the excess release of energy.[62]

1.5 Superhydrophobic Coating on Aluminium

Aluminium is a perfect material for the heat exchangers in many industries including the automotive sector. The advantages of using aluminium include low cost, high thermal conductivity, high corrosion resistance and low density with good strength. Superhydrophobic surfaces on aluminium substrates have been investigated for decades.

Ji *et al.*[66] managed to deposit micro-thick films consisting of fluorinated carbon (CFx) on the surface of aluminium substrates, using $Ar/C_2H_2/C_3H_8$

chemistry in a dual magnetron sputtering/plasma-enhanced chemical vapour deposition system. The maximum advancing contact angle observed on the treated aluminium surface was larger as 130°. Qian and Shen[41] prepared a superhydrophobic surface on aluminium by chemical etching using a mix of hydrochloric acid and acetic acid. The contact angle of aluminium surface after etching and then treating with fluoroalkysilane reached 150°, also the sliding angle was less than 10° for a 8 μL drop. Sili *et al.* [67] roughed aluminium wafers by polishing followed by boiling in water. These were then coated with a polyethyleneimine film which was reacted with stearic acid to give surfaces with contact angles of 166°. Guo *et al.*[68] modified an aluminium surface with C_9F_{20} by spin-coating for less than one minute. The resulting surface had a contact angle of 168±2°. Sarkar *et al.*[69] etched aluminium with dilute hydrochloric acid and then coated with an ultrathin rf-sputtered Teflon. By dipping the aluminium foil in a sol-gel and lowering the surface energy by chemical vapour deposition of monomolecular perfluoroalkylsilane (FAS), Xu and Wang[70] coated the aluminium with a contact angle of 160°. Menini and Farzaneh[71] created an Al_2O_3 underlayer on the surface by anodization and then deposited a tetrafluoroethylene coating onto the surface, resulting in hydrophobic surface with water contact angles of 140°.

Although many methods have been developed for preparing superhydrophobic coatings on aluminium substrates most of them cannot be used for coating compact heat exchangers because they involve steps which require open access to the surface which is incompatible with treating the heat transfer area inside louvered fin heat exchangers. The other previously reported methods involve etching which is possible with bulk aluminium but not appropriate for louvered heat exchangers since the aluminium fins are

made from foil which disintegrates under aggressive etching conditions. The main problem with coating aluminium is the stable oxide layer on the surface of aluminium makes it impossible to plate the surface directly. The zincation process is a method which was developed for industrial purposes to solve this problem. It is a simple electroless process carried out by immersing the aluminium object into a ‘zincation bath’ for several minutes after removing the oxide layer by acid and base. The process covers the surface with a microscopically rough layer of zinc. Indeed, Paluvai *et al.*[72] recently used zincation of an aluminium surface followed by lauric acid coating to achieve a superhydrophobic (150°) surface. However, such a surface will be very prone to oxidation of the zinc. In this thesis the zincation is used to create a zinc layer on the surface but this is then electrolessly reacted with a silver solution to form a rough silver surface which can then be modified with HDFT. In effect the heat exchanger is zinc plated and then treated using the standard QUB method which had previously been used to coat bulk Cu and Zn objects. Since the process involves only liquid immersion steps it allows the inside surfaces of the heat exchanger to be made superhydrophobic.

1.6 Performance of Louvered Fin Heat Exchangers

The main purpose of heat exchangers is the thermal energy exchange between the two fluids flowing on the either side of a solid portioning wall. Since the objective of the current work is to improve the performance of the system it is necessary to have method for characterising the thermal performance of a given system. There are two primary methods for defining the thermal performance: the Log Mean Temperature Difference (LMTD) method, and the Effectiveness and Number of Transfer Units ($\varepsilon - \mathrm{NTU}$) method. The method used in this work is the LMTD method which is

discussed in more detail in Chapter 2 but essentially uses the temperature difference between the input and output air to calculate the overall heat transfer coefficient and therefore the Colburn j factor.

In this work the heater exchanger to be tested is a louvered fin design so there is also a second important parameter used to characterise the performance of the heat exchanger, which is the air side pressure drop. In open architecture systems the pressure drop on the air side can be small but with louvered fin designs there will be a significant pressure drop caused by the resistance to flow through the narrow channels of the exchanger. The pressure drop is normally expressed in terms of a friction factor (f).

Several studies have been conducted on the performance of the automobile air conditioner evaporators in the context of full AC systems under various operating conditions. For example, Ratts and Brown[73] used experimental methods to analyze the coefficient of performance (COP) of automobile AC system, this parameter characterises the performance of the entire system. In their work, relationships were developed for the relationships between the COP and the compressor and vehicle speed. Gu *et al.*[74] experimentally determined the two-phase flow inside an evaporator and noted its effect on heat transfer performance of an evaporator. G.H. Lee and J.Y.Yoo[75] have carried out performance analysis and simulation of an automobile air conditioning system. A computer program was developed to analyze the performance of an automobile evaporator based on the overall heat transfer coefficient and pressure drop which were obtained experimentally. This program gave simulations of evaporating pressure, evaporating capacity and outlet air temperature if the inlet air temperature and humidity, air flow rate, outlet refrigerant superheating, inlet refrigerant quality and mass flow rate were given. Jabardo and Mamani [76] developed a

model for evaluation of evaporators in automobile AC systems based on the assumption that thermal resistance due to wall conduction, contact, and fouling are negligibly small.

Although studies on full systems are extremely useful it is very difficult to investigate the effect of changing design characteristics of heat exchangers on full systems so this optimisation work is typically carried out on systems where the performance of just the heat exchangers, rather than a whole system, is measured. For example, Sanaye *et al.*[77] investigated thermal models of laminated evaporators compared with mini-channel evaporators. The ε - NTU method was used for thermal analysis in their report. Two wet and dry cases of air flow through the evaporator were investigated. The pressure of the laminated plate fin type of evaporator was measured experimentally due to the complicated plate-fin geometry and the modelling results were then compared with the experimental results. Their modelling results had a good accuracy in comparison with the experimental tests.

Similarly, a large number of studies have been carried on to analyze the heat transfer and pressure drop characteristics of compact heat exchangers. Springer and Thole[78] performed numerical and experimental studies on the flowfield measurements of louvered fin configurations under different Reynolds number. Chang *et al.*[79] performed experimental studies on the air-side characteristics of louvered fin heat exchangers and made correlations for j and f factors. Man-Hoe Kim *et al.*[80] have carried out experimental studies on the air-side heat transfer and pressure drop characteristics for multi-louvered fin heat exchangers with different designed geometries. Wei-Mon Yan[81] have examined 36 louvered fin heat exchangers with different geometries and performed heat transfer and pressure drop

characteristics. They showed the performance of heat exchanger with plots of friction factor f and Colburn factor j against Reynolds number in the range 300-2000.

Importantly in the current context, some reports have focused on the retention of condensate on heat exchangers. Kim *et al.*[82] investigated the condensation of different fin and tube heat exchangers. It was found that condensate blockage can increase the air side pressure drop and decrease heat transfer. Osada *et al.*[83] tested evaporators under wet conditions and found that the expected heat transfer enhancement by the louver effect did not occur because of the condensate trapped between fins. They also reported that a hydrophilic coating promotes the drainage of condensate. Yin *et al.*[84] investigated the retained water on plain–fin and wavy - fin heat exchangers under wet conditions and developed a model to predict the condensate retention.

There is only very limited research on the performance of hydrophobic coated heat exchangers. Sir[85] found that evaporators with hydrophobic coating have about 5 % higher dehumidification efficiency compared to hydrophilic ones under high inlet relative humidity.

Liu[86] investigated the impact of surface wettability on different heat exchangers. A wide range of surface wettability from hydrophilic to hydrophobic was covered with contact angle from 30° to 110° their results showed the hydrophobic surfaces did not help decrease the air-side pressure drop for very compact heat exchangers by reducing the amount of condensate retention. Liu and Jacobi[87] concluded that under dry conditions there is not much difference in the Colburn j factor (heat transfer), f - factor (pressure drop) of uncoated and hydrophobic fin surfaces (θ = 110°) for different Reynolds numbers. Under wet conditions and for different Reynolds

number, the Colburn j - factor of the hydrophobic surface was about 13 % lower and f - factor is around 36 % to 48 % higher compared with an equivalent uncoated surface. The report also indicated that the hydrophilic coated heat exchanger showed good performance with lowest pressure drop and highest heat transfer coefficient.

There is even less data on the performance of heat exchangers with superhydrophobic coatings (as opposed to hydrophobic coatings) compared with bare heat exchanger. Preston *et al.*[88] tested the water condensation heat transfer performance for the copper tubes with CuO superhydrophobic coatings (θ = 170°), hydrophilic surface (θ = 14.6°) and hydrophobic surface (θ = 123.4°). The results shows that the condensation heat transfer coefficient under low supersaturation of jumping mode which happened on the superhydrophobic surface is around 30 % higher than the dropwise model and 5 times of the filmwise mode occurred on the hydrophilic surface. No experiments with superhydrophobic coated louvered fin heat exchangers have been reported. In contrast, the performance of hydrophilic heat exchangers has been studied by several groups. Wang and Chan[89] compared the heat transfer coefficient and pressure drop of hydrophilic coated and uncoated louvered fin heat exchangers. They found under wet condition the hydrophilic coating has negligible effect on the sensible heat transfer coefficients but the pressure drops are much lower (15 - 40 %) than the bare heat exchanger. The same conclusion was reported by Hong *et al.*[90] and Wang *et al.*[91],Kim and Jacobi[82] reported hydrophilic plate-fin-and-tube heat exchangers retained less condensate in comparison to that of bare heat exchanger for all the velocities tested. Hong *et al.* found that a reduction of 25 % of pressure drop for hydrophilic louvered heat exchangers compared with uncoated heat exchangers. The hydrophilic

coating results in the reduction of condensed water on the heat exchanger which may increase the heat transfer coefficient for compact heat exchangers.

1.7 Research Aims

The main aim of this research is to apply a superhydrophobic coating onto automobile evaporators which have a louvered fin design. The coating method was developed in previous work but much more extensive work is needed to scale up the process so it can be used to routinely coat compact heat exchangers. Similarly the properties of the coating when applied to a heat exchanger surface need to be properly investigated. An alternative method to coat stable superhydrophobic coating on the surface of the heat exchanger by applying superhydrophobic powder will be investigated.

A new testing apparatus will be built to measure the heat exchanger performance. The pressure drop and heat transfer of untreated and superhydrophobic coated heat exchanger will be analyzed and compared to see the impact of surface modification on heat exchangers. Superhydrophilic coated heat exchangers will be tested to make comparisons.

A related aim of this research is to investigate the effect of superhydrophobic coating on the amount of condensate which is retained between fins during operation below the dew point. This will be tested independently through dynamic dip testing which is the standard method for measuring water retention in various designs of heat exchangers.

Chapter 2 Experimental

Chapter 2 Experimental

2.1 Instrument

2.1.1 Contact Angle Measurement

The most widely used method to measure contact angle is direct measurement of the tangent angle at the liquid-solid and liquid-gas interfaces on an image of a liquid drop. The image may be recorded using either a still or video camera. The system applied in this report was a First Ten Angsttoms FTA1000B Drop Shape Instrument which was based on the direct measurement by telescope and goniometric analysis. Automatic contact angle analysis, system control and data export was provided by FTA32 software.

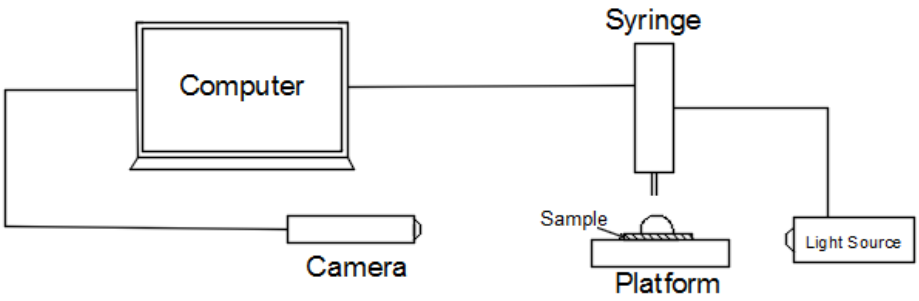

Figure 2.1 FTA1000B Contact Angle Measurements

A drawing of the equipment structure is shown in Figure 2.1. An adjustable horizontal platform was used to mount the tested sample. The syringe pump which was driven by a stepper motor was placed above the platform to form the sessile drop. A LED light source was arranged to illuminate the drop from the opposite direction of the camera to improve

image by allowing the drop to be photographed against a bright uniform background created by the LED-illuminated screen. The image of the liquid was captured by a CCD camera. FTA32 software was used to fit the baseline and analyze the captured image to obtain the resulting contact angle.

The automatic fit function of the software does not work accurately for angles greater than 120°.[92] In this work, the baseline was selected by the user manually and several points on the drop were marked by the user. The contact angle was then calculated by the software. The advantage of the system is the simplicity and the speed of obtaining the results. However, measurement of small substrates can give errors due to irregularities or impurities on the substrate, since the droplets roll off the parts with the highest contact angle and may fall off the edge while the droplets which are left, almost by definition, are those which are pinned at the least hydrophobic parts of the surface. In addition, the measurement relies on the input from the operator for accuracy and reproducibility which could lead to significant error and inconsistency between multiple users. Therefore, when using the instrument consist operating methods and multiple tests are needed to give reliable and accurate results.

2.1.2 Scanning Electron Microscopy and Energy Dispersive X-Ray

The surface coating was analyzed by SEM (scanning electron microscopy) and EDX (energy dispersive X-Ray analysis). The SEM uses a focused beam of high energy electrons to generate a variety of signals at the surface of solid specimens. The signals that derive from electron-sample interactions reveal information about the sample including external morphology, chemical composition, crystalline structure and orientation of materials making up the sample. The instrument used was an FEI Quanta

FEG 250 SEM at an acceleration voltage of 20kV under high chamber vacuum with standard SEM copper tape as the background. Scanning electron micoroscopy with energy dispersive X-Ray analysis is one of the best known and most widely-used of the surface analytical techniques. An Oxford Instruments EDX system was attached to the SEM used in this work. The data generated by EDX analysis consists of spectra showing peaks corresponding to the elements making up the composition of the sample being analyzed. Elemental mapping of a sample and image analysis are also possible.

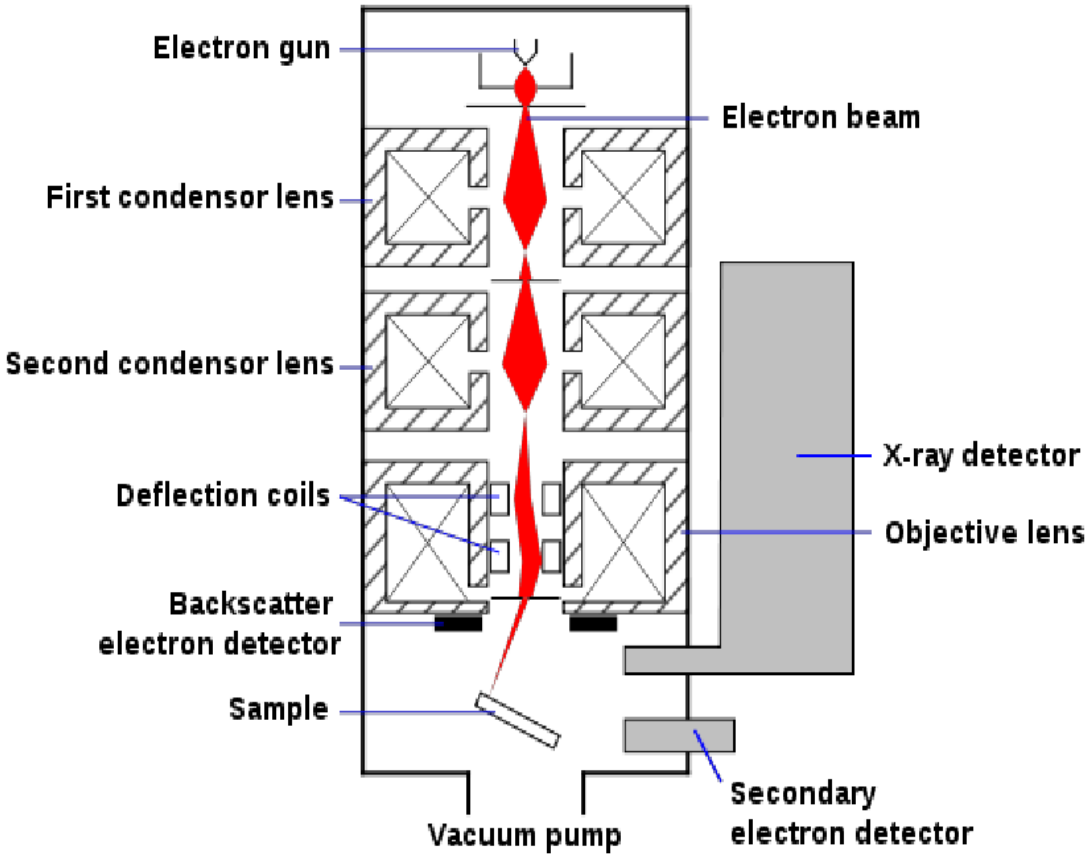

Figure 2.2 Schematic of an SEM.[93]

2.2 Superhydrophobic Coating Method

The method of superhydrophobic surface coating used in this research was first reported by Bell *et al.*[44] This simple and fast method was chosen to coat the evaporators from automobile air conditioning systems. The original electroless coating method was based on coating solid copper or zinc substrates while the evaporators were made of aluminium so a method for depositing a superhydrophobic coating on aluminium which was developed by J.McCracken in QUB was used.

In this method, the aluminium piece was cleaned in 10 % sodium hydroxide for 10 s and then cleaned in 30 % nitric acid for 10 s (rinsed with distilled deionzied water and dried after each step). Then aluminium was dipped into zincating solution for 120 s to 150 s, rinsed and dried. The zincating solution contained 120 g L^{-1} sodium hydroxide, 4 g L^{-1} zinc oxide, 1 g L^{-1} sodium nitrate and 50 g L^{-1} potassium sodium tartrate tetrahydrate. The reactions are shown below:

$$Al_2O_3 + 2\ NaOH + 3\ H_2O \rightarrow 2\ NaAl(OH)_4 \qquad (2.1)$$

$$2\ Na_2Al(OH)_4 + 2\ Al \rightarrow 2\ NaAl(OH)_4 + 4\ NaOH + 3\ Zn \qquad (2.2)$$

The zincated aluminium object was then immersed in 0.01 M silver nitrate for one minute. This caused electroless deposition of Ag as shown below：

$$Zn + 2\ Ag^{+} \rightarrow Zn^{2+} + 2\ Ag \qquad (2.3)$$

If the object was not completely black a second coating step was used. This involved rinsing the object with water and then dipping it into silver nitrate for another 40 s. The final step was to dip the silvered object in a 0.001 M solution of HDFT

(3,3,4,4,5,5,6,6,7,7,8,8,9,9,10,10,10-heptadecafluoro-1-decane-thiol, structure shown in Figure 2.3) in dichloromethane for 5 to 10 minutes. Superhydrophilic samples were treated with 6-mercapto-1-hexanol as the final functional chemical in the same process.

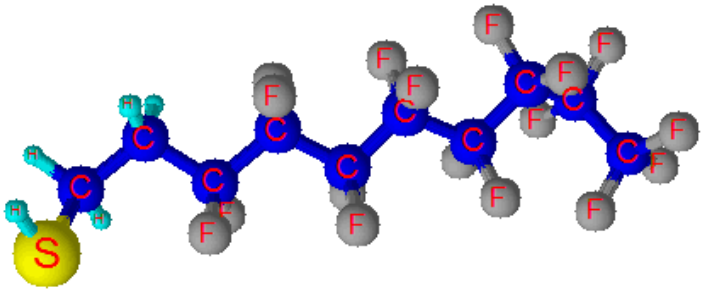

Figure 2.3 Structure of HDFT.

2.3 Methodology

When air-and-water heat exchangers operating under typical moist conditions, the dominating thermal resistance is on the air side which make up 98 % of total thermal resistance.[78] In this work, tests were conducted to compare the heat transfer performance of different coated heat exchangers in the system. The calculation was based on the heat transfer at the air side. A log-mean-temperature-difference method was used to analyze the heat exchangers. Since there was no completely sealed test apparatus available in the lab the overall heat transfer coefficient was used to analyse the performance of the coated heat exchangers and outlet air velocity was used as the reflection of pressure drop.

2.3.1 Heat Transfer Rate

The basic heat transfer parameter was calculated based on the principle of

energy conservation equations. The basic equation is shown in equation (2.4).

$$Q = m * c_p * \Delta T \quad (2.4)$$

Where m is the mass of substrate; c_p is the specific heat capacity; ΔT is the change in temperature. Moist air is a mixture of dry air and water vapour. The enthalpy of moist and humid air includes the enthalpy of the dry air, the sensible heat, the enthalpy of the evaporated water and the latent heat. For the air and coolant flow, air side heat transfer rate calculation equation was given by Kim and Bullard.[94] The data used in equation is based on measurements at the air-side inlet and outlet test sections.

$$Q_a = m_a\left[C_{p\,air}\left(T_{a1}-T_{a2}\right)+C_v\left(H_1T_{a1}-H_2T_{a2}\right)\right]+h_g m_a(H_1-H_2) \quad (2.5)$$

Where m_a is the mass flow rate of air, $C_{p\,air}$ = 1.006 (kJ kg^{-1} K^{-1}) is the specific heat of dry air, C_v = 1.84 (kJ kg^{-1} K^{-1}) is the specific heat of vapour, T_{a1} and T_{a2} are the inlet air temperature and the outlet air temperature respectively; H_1 and H_2 are the measured humidity ratio of inlet and outlet air; h_g is the latent heat of vaporization of water (2501 kJ kg^{-1} at 0 ^oC).

The mass flow rate of air depends on the inlet air speed and front area.

$$m_a = V_1 * A * \rho \quad (2.6)$$

Where V_1 is the inlet air velocity of the tunnel and A is the tunnel area applied on the system. The density of humid air was different from the density of dry air at same temperature; it varies with water content and temperature. When the temperature rises, increased molecular motion results in expansion of volume and a decrease of density. The equation (2.7) to calculate moist air density is given below.

$$\rho = \frac{P - p_w}{R_a * T_{a1}} + \frac{p_w}{R_w * T_{a1}} \quad (2.7)$$

Where P is the total pressure (assumed to be 101 kPa); $R_a = 287.05$ J $kg^{-1}K^{-1}$ is the specific gas constant of dry air and $R_w = 461.495(J\ kg^{-1}K^{-1})$ is the specific gas constant for water vapour.

p_w is the partial pressure of water vapor calculated from equation (2.8).

$$p_w = RH * p_{wo} \quad (2.8)$$

Where the p_{wo} is the saturated vapour pressure given from steam table (shown in Appendix A) at certain temperature; RH is relative humidity measured by humidity data logger during the experiment.

H_1, H_2 represents the ratio humidity which was calculated by the equation (2.9).

$$H = \frac{Mw * p_w}{Ma\ (P - p_w)}\ kg\ kg^{-1} \quad (2.9)$$

Where Mw is the molecular weight of water; Ma is the molecular weight of air. For air-water system, $p_w << P$, the humidity is approximated by

$$H = \frac{18 * p_w}{29\ (P - p_w)}\ kg\ kg^{-1} \quad (2.10)$$

2.3.2 Overall Heat Transfer Coefficient

A log-mean-temperature-difference (LMTD) method was employed to analyze the heat transfer performance. To obtain air-side overall heat transfer coefficient, firstly the LMTD was calculated. The LMTD for counter flow is:

$$LMTD = \frac{(T_{a1}-T_{w2})-(T_{a2}-T_{w1})}{\ln(\frac{T_{a1}-T_{w2}}{T_{a2}-T_{w1}})} \quad (2.11)$$

The overall heat transfer coefficient represents the overall ability of heat transfer from one fluid to another. It is a function of the flow geometry, fluid properties and material composition of the heat exchanger. In a heat exchanger, the relationship between the overall heat transfer coefficient (U) and the heat transfer rate (Q) is given below.

$$UA = \frac{Q_a}{LMTD} \quad (2.12)$$

Where A is the total air side surface area and Q_a is the heat transfer rate. UA is the overall heat conductance and $\frac{1}{UA}$ can be seen as the total thermal resistance. In a wind tunnel test, the total resistance is made up of three resistances: water side, tube wall, and fin side.

$$\frac{1}{UA} = \frac{1}{h_t A_t} + \frac{1}{\eta h A_0} + R_w \quad (2.13)$$

Where h and h_t are the heat transfer coefficients of air and inside of the tubes, respectively. A_t and A_0 are the total surface areas of the air side and the interior of the tubes, respectively. Since the heat transfer area on the interior of the tubes and on the exterior in cylindrical geometry are same for coated and uncoated heat exchangers, the overall thermal conductance (UA) can be used to describe heat exchanger performance. For louvered fin heat exchangers, the equations describing the performance of the overall system are dependent on structure of fins. However, since the object of this research is to compare the effect of superhydrophobic coating on evaporators and the louvered fins on heat exchangers in these experiments

are exactly same, the effect of the structure of the fins in the calculations of the effects of the coating cancel.

2.3.3 Air-side Velocity Difference

The pressure drop across the air-side of heat exchanger is an important factor when analyzing the performance of heat exchanger. The total pressure drop through the core depends on the geometric parameters, the type of fluid types and the thermodynamic properties.[95]

For a completely sealed system, pressure drop can be directly measured by pressure taps and recorded during the operation. Since the system used in this project was not well-sealed, the measurement of pressure drop was replaced by measuring the difference between inlet and outlet air velocity.

2.3.4 Construction of the Heat Transfer Test System- Overview

A system was built in order to mimic the operating conditions for evaporators in car air conditioning system. Normally, closed-loop wind tunnel systems are used to determine the retained condensate and heat transfer performance of the heat exchangers but because of the limitation of lab equpiment and time, a simpler system was used in this study.

In previous work at QUB, a tray drier was used to create a simple water-to-air heat exchange system. The chiller was connected to the tested heat exchanger which was fixed inside the tunnel of the tray dryer. Air was drawn into the tunnel by an axial flow fan while air temperature and humidity were controlled at the entrance of the tunnel to supply the required hot and

humid air. Energy usage and temperature reduction performance were tested by tray dryer system but in this system the heat exchanger was very inaccessible during operation and was extremely difficult to measure the amount of water condensation occurring.

A more accessible compact system was constructed for the current project. Figure 2.5 shows the schematic of the test apparatus and Figure 2.6 is a photograph of test system in the laboratory. The system was designed to draw hot and moist air over the finned side of the evaporator while circulating cold water through its cooling tubes. In the system, a chiller was used to cool and pump cold water continuously through the heat exchanger, this differs from actual automotive air conditioning where the coolant is fluorocarbon or equivalent but here water was used as the coolant since it eliminated the need to pump volatile refrigerant around the system. The chiller was set to operate with the target temperature at 5 ^{o}C. In this condition, the entire heat exchanger's temperature is below the dew point temperature of inlet air.

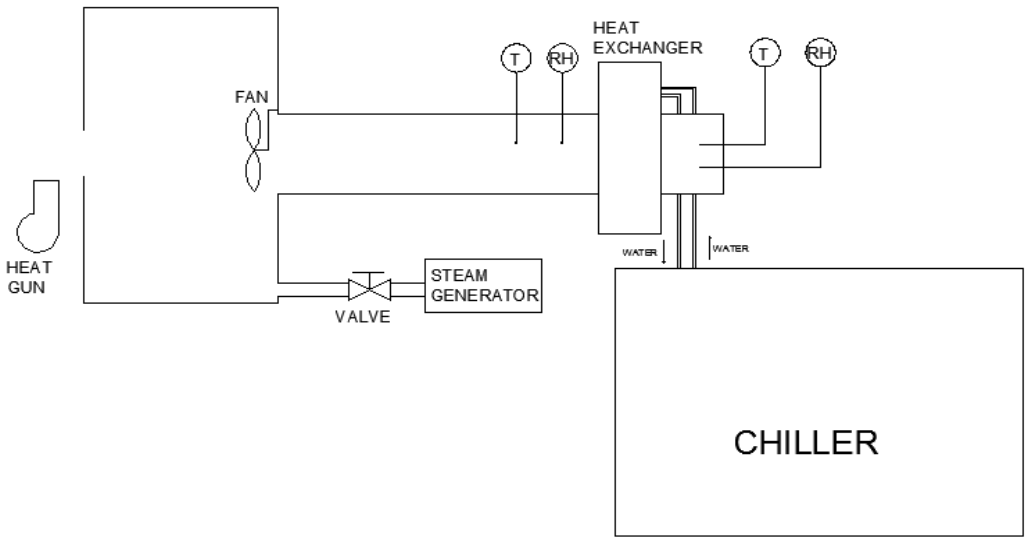

Figure 2.5 Schematic of the test apparatus.

A mixing chamber was used to mix hot air (generated by a heat gun heating air at entrance of chamber) and moist air (from a steam generator connected to the chamber). A valve in the tube connecting the chamber to the boiler was used to control the amount of steam being mixed into the airstream and therefore the humidity of inlet air. Air from the mixing chamber was directed to the heat exchanger with a flexible tube. The air flow was determined by a fan inside the chamber and was measured by digital air flow meter. An Aim-TTi® EX4210R power supply was used to supply power on the fan. Air flow rate was adjusted by the voltage on the fan and was measured by digital air flow meter. Inlet/outlet air temperature and relative humidity were recorded by thermocouple data logger and humidity data logger, respectively. Insulation covered the cooling pipe and steam pipe to cut down heat loss and prevent or reduce damage to electronic equipment.

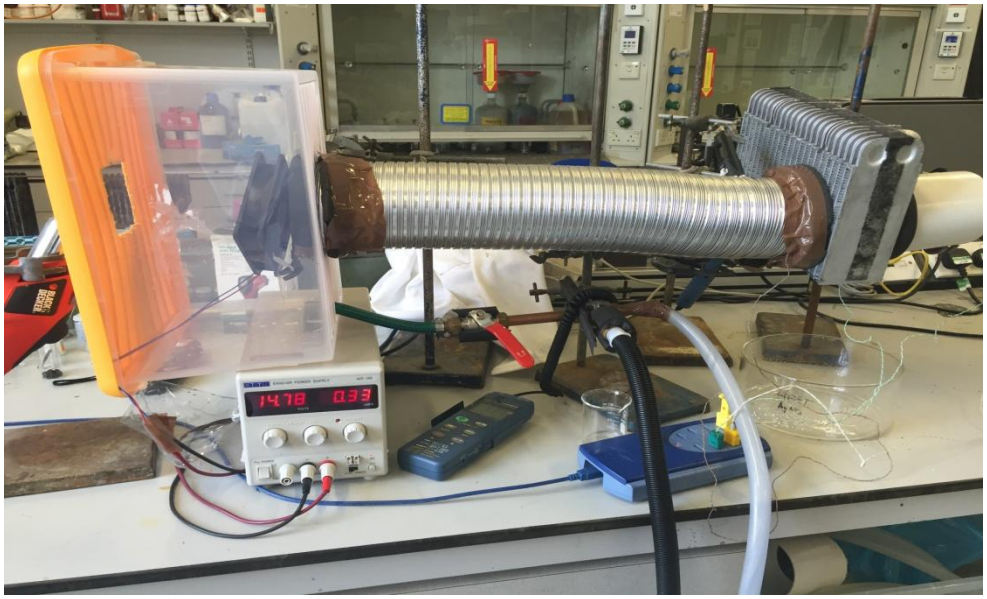

Figure 2.6 Photograph of the test apparatus.

2.3.5 Detailed Description of the Components of the test System

2.3.5.1 Louvered Fin Heat Exchanger

Louvered fin heat exchangers are widely applied in power generation, air conditioning, and heating and evaporation. The louver fin pattern is one of the most effective enhanced extended surfaces available and is created by cutting the sheet metal of the fin at intervals.[96] Louvered fin heat exchangers are chosen as evaporators or condensers for low cost and low heat exchanger volume with high heat transfer surface area, which makes them particularly suitable for automobile air conditioning systems.[51] A variety of materials can be used in the design of compact heat exchangers, including aluminium, stainless steel, copper and carbon steel. Aluminium is considered to be the best core material because of its ability to provide high heat transfer efficiency combined with low weight.[51]

The louvered fin flat tube heat exchanger used in this research was produced by Nissens as the evaporators (Model 92183) used in automobile air conditioning systems. The parameters of the heat exchanger are shown in Table 2.1. In use, the hot air flow through the fins is chilled by the coolant running through the flat tube which means that louvered fins effectively increase the velocity of the working fluid relative to the elemental flat-plate surfaces.[97]

Table 2.1 Parameters of louvered fin heat exchanger used in this work

Flow depth	36 mm	**Tube depth**	28 mm
Louver angle	30°	**Fin length**	7 mm
Louver pitch	1 mm	**Fin height**	10 mm
Tube pitch	12 mm	**Fin pitch**	1.5 mm
Total Length	272 mm	**Total Width**	212 mm

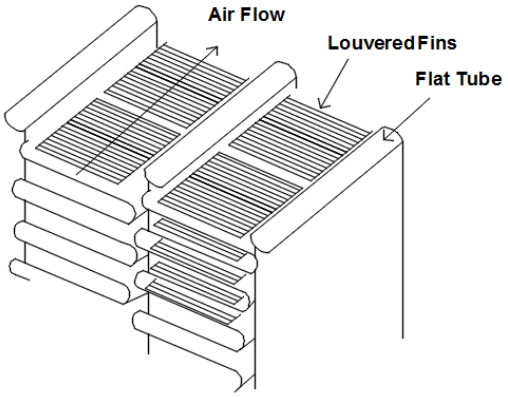

Figure 2.7 Flow direction of louvered fin heat exchanger.

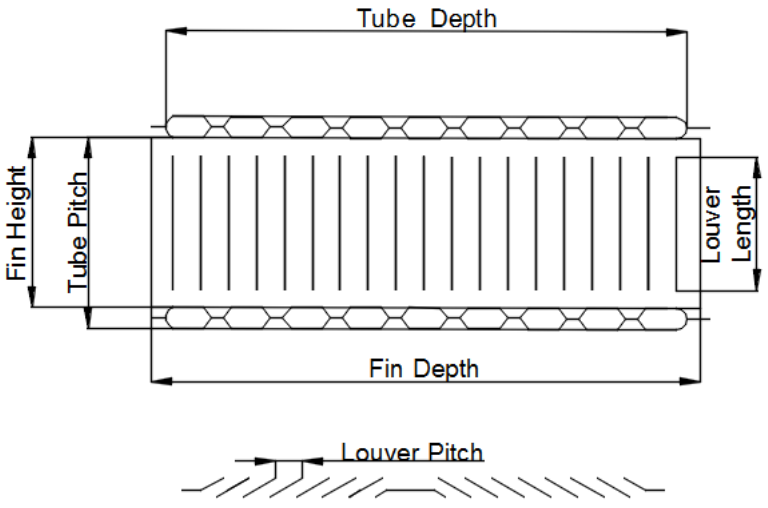

Figure 2.8 Definitions of the geometrical parameters for a louvered heat exchanger.

2.3.5.2 Chiller

The water chiller used in the system was MTA® M10 Water Chiller which is a high capacity chiller designed to supply continuous cold water as coolant. The design criteria and general information are given in Table 2.2.

Table 2.2 Specifications of the water chiller used in this work.[98]

Application	Process Cooling	
Thermal duty	4.4 kW	
Fluid type	Water/Glycol solution	
Refrigerant	R407C(23 % Difluoromethane(R32); 25 % Penrafluoroethne(R125); 52 % R134a)	
Cooling fluid supply temperature	15.0 ℃	
Cooling fluid return temperature	20.0 ℃	
Cooling fluid flow rate/pressure	12.6 ltr/min	
Ambient air temperature	Minimum 5 ℃	Maximum 40 ℃
Evaporator water inlet temperature	Minimum 5 ℃	Maximum 35 ℃
Evaporator water outlet temperature	Minimum 0 ℃	Maximum 30 ℃
Pump head	4/0 bar	

In operation, the refrigerant is pumped by the compressor to the condenser. The compressor relay is active to maintain a given temperature value, which is established by the set-point temperature. The compressor is active to keep the temperature at a certain value established by the set-point. Hysteresis Hy is automatically added to the set-point (see Figure 2.9). As the coolant circulated the temperature rises and when it reaches the set-point + hysteresis, the compressor is started and it then runs until the temperature value returns to the set-point value. During the experiment, when the outlet water temperature of chiller reached 5 ^{o}C, the chiller stopped cooling but it continued to pump the water around the system. When the temperature rose to 9 ^{o}C the chiller would restart and the cycle was repeated.

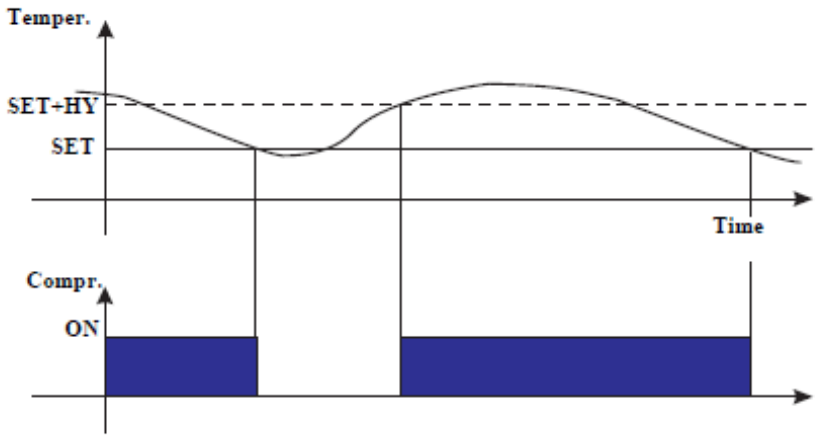

Figure 2.9 Temperature control of the compressor in the chiller used in this work.[98]

2.3.5.3 Measurement Equipment

Air Flow Measurement

In the initial stages of the work an Extech® 45170 Pocket Hydro-Thermo-Anemometer-Light 4-in-1 Environmental Meter was used to measure the air velocity. The resolution of the 4-in-1 experimental meter is 0.1m s^{-1} with an accuracy of ± 3 %. During the experiments, under some of the operating conditions test, the outlet air velocity was found to be lower than the minimum value that the meter could measure. Therefore a higher performance of airflow meter with higher accuracy and larger operating range (TSI® AIRFLOW LCA501 rotating vane Anemometer) was used in subsequent experiments. The accuracy and resolution of this rotating vane anemometer was ± 1.0 % of reading ± 0.02 m s^{-1} and 0.01 m s^{-1}, respectively, while its minimum velocity was 0.1 m s^{-1}.

Humidity Measurement

Two types of humidity meter were used in this system. OMEGA®

OM-EL-USB-2-LCD data loggers were installed at the inlet tunnel and outlet tunnel to record the relative humidity of air. The internal resolution and accuracy of this data logger were 0.5 % RH and 2.25 % RH, respectively. Since it normally takes several minutes to ensure the OMEGA® data logger has reached the thermal equilibrium with its surroundings the system was allowed to equilibrate for 5 minutes before readings were recorded. The humidity was recorded at ten second intervals and exported by EasyLog® software. An OMEGATTE® HH314A Humidity Temperature Meter with better resolution (0.1 % RH) was placed at the inlet tunnel as a sensor to control the inlet relative humidity.

Controlling the Properties of the Input Air

The temperature and humidity of the inlet was set to the required values by heating and adding steam directly at the entrance to the tube which was connected to the evaporator being tested. In the initial experiments it was found that the measured temperature and relative humidity were not stable during the experiment. The failure to control the condition of the inlet air humidity and temperature was due to the heated air and steam being poorly mixed before it was blown into air side of heat exchanger. Inspired by wind tunnel systems, a mixing chamber was added to ensure the steam and heated air were well mixed and achieved stable required temperature and humidity before being passed through the exchanger. A 23 cm x 32 cm x 20 cm plastic box was used to mix the air with a 7 cm x 8 cm entrance hole where the hot air was blown in and another small entrance for the steam pipe on the opposite side.

A Black&Decker® KX1682 heat gun was used to increase the air temperature to the required value. The temperature of the air entering the

mixing chamber was adjusted by changing the distance between the heat gun and air entrance.

Steam was generated by an Earlex SS125 ‘Maxisteam’ wallpaper steamer. At first, a 3-way switchable Y piece plastic garden hose pipe connector was used to control the steam flowing into the chamber. The connector could control the flow direction but was not sufficiently air tight to allow proper control of the steam, so it was replaced by a copper T piece and a separate brass ball valve which was designed for domestic plumbing and had significantly better performance. A drawing of connections is given in Figure 2.10, which shows that the copper pipe with T joint was connected to the steam generator. One exit side of the pipe was fitted with a ball valve to control the amount of steam which was extended to the chamber to supply required humidity. The other side of T piece was exposed to the environment in order to discharge excess stem and prevent pressure build up in the steam generator.

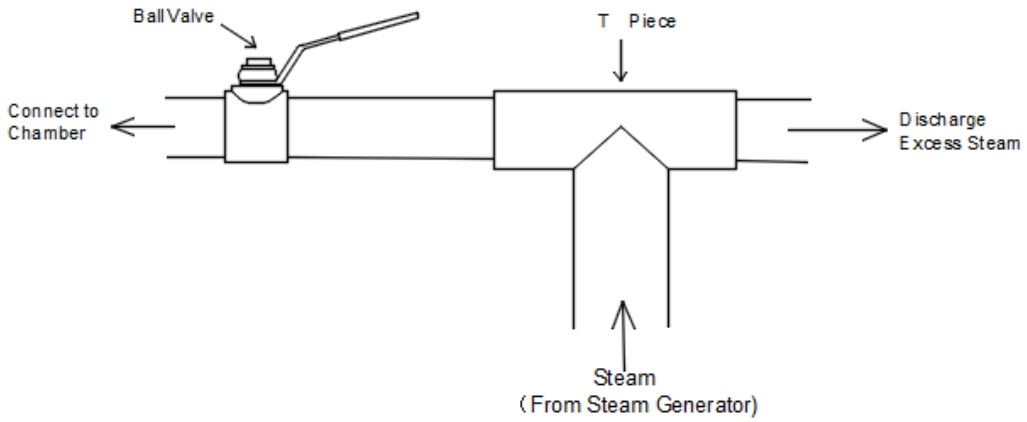

Figure 2.10 Sketch of the system used to control of the inlet steam.

The test experiments were run for 40 minutes. However, since the steam generator needed to be refilled with water at regular intervals the heat gun was operated for 10 minutes and there was then a 3-5 minute break

during which the steamer was refilled before the experiment was restarted. The outlet air velocity was recorded every 15 minutes to reflect the condensation retention performance. A container was positioned under heat exchanger to collect condensation running off the evaporators.

During the initial runs with the test system it was found that an effective air conditioning system was built up. The inlet air could be cooled from 33 °C to less than 10 °C. The relative humidity of the inlet air could be controlled from 40 % to 70 % (at around 33 °C). During the experiment, the outlet air velocity of superhydrophobic coated evaporators was found to decrease with time due to blockage of fins caused by condensation. This was unexpected since the superhydrophobic surfaces would not be expected to hold water. This was found to be partly due to degradation of the surface (discussed below) but also partly due to the geometry of the exchanger under test. Dip tests were therefore used to further investigate the condensation discharge ability of the coated and uncoated exchangers.

Chapter 3 Results and Discussion

Chapter 3 Results and Discussion

3.1 Surface Coating

The first step in this project was to prepare evaporators with superhydrophobic surfaces. A surface coating method which has been used for treating small (3 cm^2) flat specimens of aluminium was developed and used in previous work in QUB. However, for the work in this thesis the object to be coated was the evaporator from an automobile air conditioning system which has a complex, louvered-fin design. Although in principle the existing process should be easy to scale up since it involved only immersion, rinsing and drying steps, it was found that scaling up from coating small pieces to full heat exchanger was not straightforward and initial attempts to simply follow the established procedure gave poor results where the coating was patchy with both hydrophobic and hydrophilic areas.

There are many potential reasons for the failure of coating process but the most likely sources are in the zincating rather than electroless Ag deposition which is extremely straightforward and occurs spontaneously in a few seconds with flat zinc substrates. Firstly, the immersion time of zincating process could affect the adhesion of zinc layer on Al, the optimum time for zincating flat pieces of Al was found to be 120 s to 150 s by J.McCracken in his PhD work but this may not transfer directly to larger complex objects. Similarly the zincating solution needs to have sufficient Zn available to provide a good coating. Indeed, in the first test runs a zincation solution which was left from previous studies was used and this was completely unsuccessful. However, even with a fresh solution the zincation step may give a coating which visually appears patchy and incomplete. This was

solved by using a second immersion in the zincation solution. It is not clear whether the improved coating on second immersion is simply due to improved mass transfer of the solution but whatever the reason the results given by a second coating step mean that it should be carried out if there is any doubt.

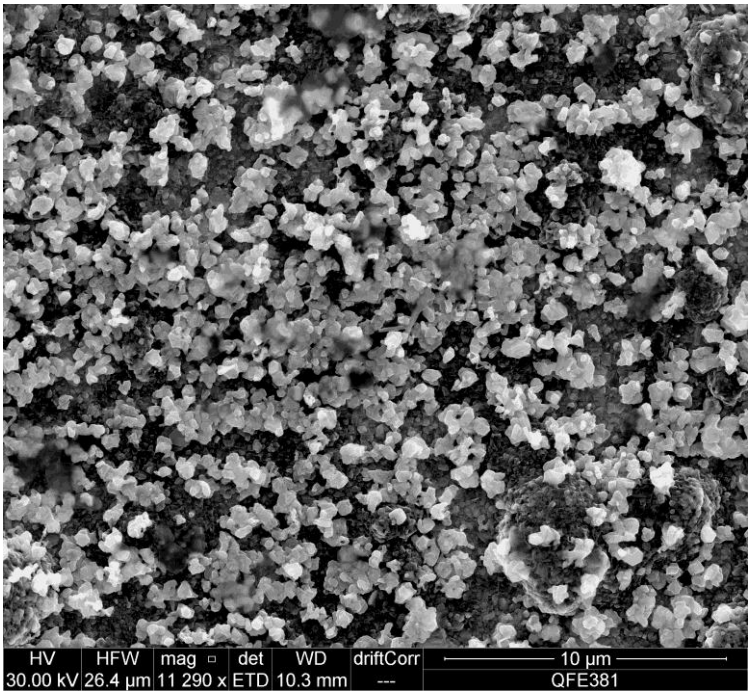

Figure 3.1 (a) SEM image of an aluminium fin after single zincation treatment for 150 s.

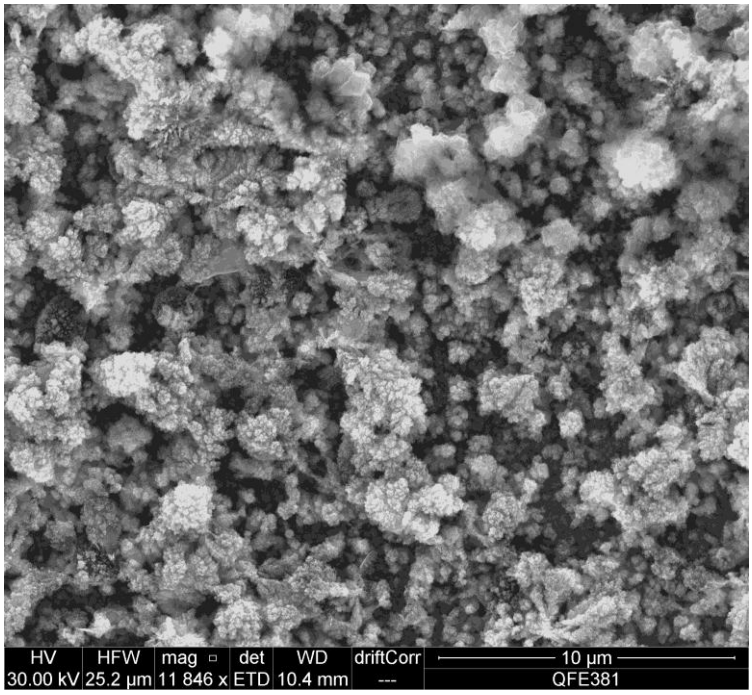

Figure 3.1 (b) SEM image of zincated aluminium fin after silver deposition.

The colour after zincation step was even after successful zincation the subsequent silvering and HDFT steps did not initially give superhydrophobic coatings on the heat exchangers. This was found to be due to two small important effects. Firstly, the zincating solution is highly alkaline, so the step where the heat exchanger is rinsed after the zincating process is important since any residual solution can affect the subsequent silvering process. With small test pieces this rinsing is easy but with the heat exchanger initial attempts at coating where the exchanger was washed under running distilled deionzied water were not sufficiently thorough to rinse the solution out of the cavities in the heat exchanger. This resulted in poor coating performance in the final product. This was solved simply by the more extensive rinsing described in the Methods section.

Secondly, it was found that if the heat exchanger was not dried completely after silver deposition, the water layer in the wet part blocked any

contact between the dichloromethane HDFT solution and the deposited silver coating, preventing the reaction with HDFT which lowers the surface energy (Figure 3.2).

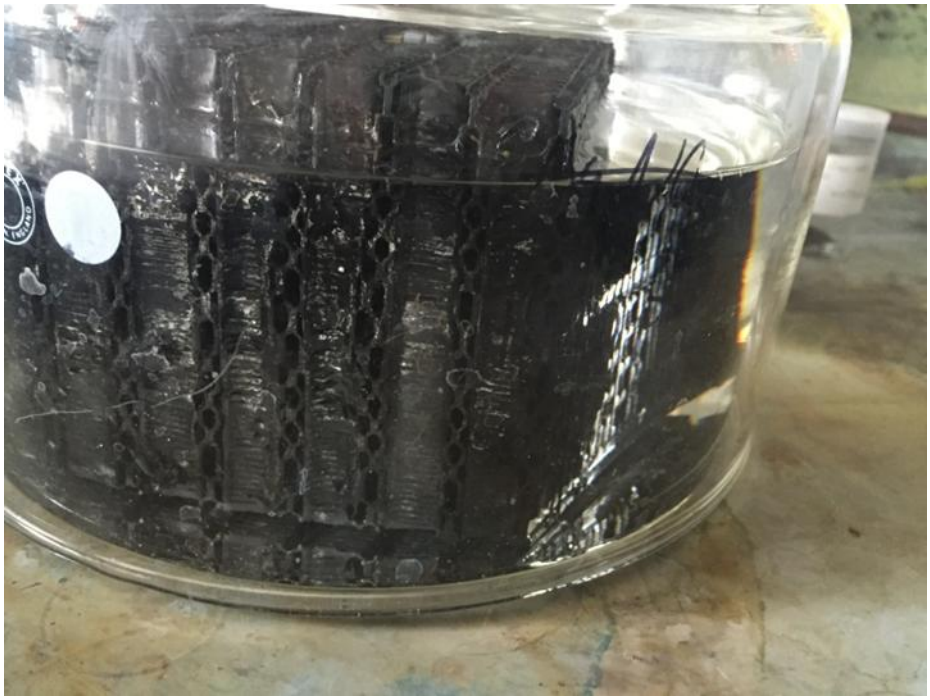

Figure 3.2 Coated heat exchanger immersed in dichloromethane showing reflective ‘silvery’ area caused by residual water on the exchanger.

The structure of louver fin heat exchanger is complicated, so the external surfaces may be dry while the inside may not be completely dry, even after several minutes. There are two solutions to this problem. The first one is to change the solvent from dichloromethane (DCM) to a water-miscible solvent such as ethanol. This would allow the HDFT solution to reach areas which contain residual water. Unfortunately switching solvents would also have introduced the problem that thiol adsorption rate are very different in different solvents so slower kinetics might have occurred. A simpler solution was to rinse the heat exchanger with a solvent that was miscible with both water and DCM so that the bulk of the surface would be

contacted by DCM solution, albeit mixed with the solvent residue. In practice, the heat exchanger is washed with distilled deionised water and dried after reacting with silver nitrate. It was then washed with ethanol and dried before immersion in HDFT. This method was found to be successful but in any case where the HDFT coating was not complete it was easy to use a second dip step if required.

Implementation of these simple changes allowed superhydrophobic coating of the exchangers to be carried out routinely to give highly hydrophobic surfaces, as shown in Figure 3.3.

Figure 3.3 Water drops supported on top of the fins in a superhydrophobic evaporator.

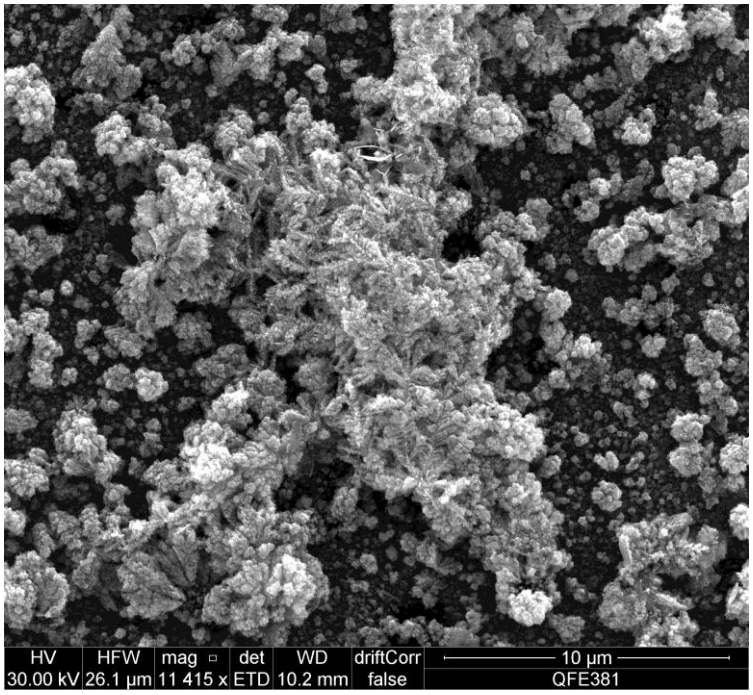

Figure 3.4 SEM image of aluminium piece after HDFT treatment.

3.2 Dynamic Dip Test

3.2.1 Introduction and Experiment

For many years dynamic dip tests have been used as a fast and simple way to assess the condensate drainage behaviour of the air-side surface of heat exchangers. It has been reported that heat exchangers which hold more water during a dip test tend to hold more condensate in a wind-tunnel experiment.[99] Based on this observation, dynamic dip tests are now well established as a reliable and valid method for assessing the condensate drainage behaviour from the airside surface of various designs of heat exchangers.

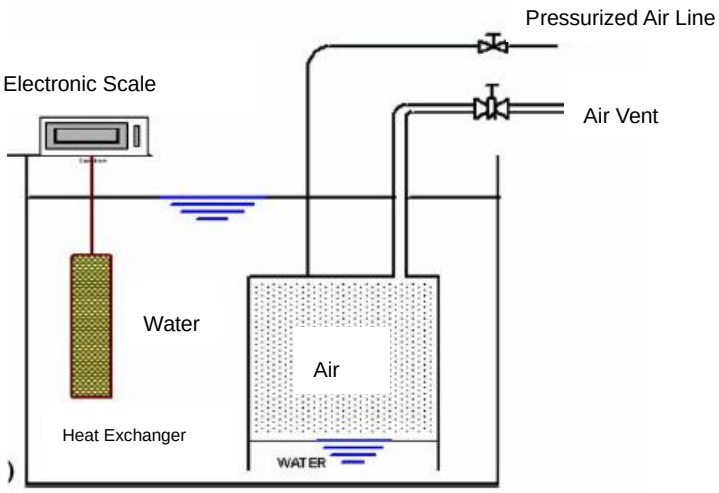

Figure 3.5 (a) Schematic diagram of a system that can be used for dynamic dip testing.[99]

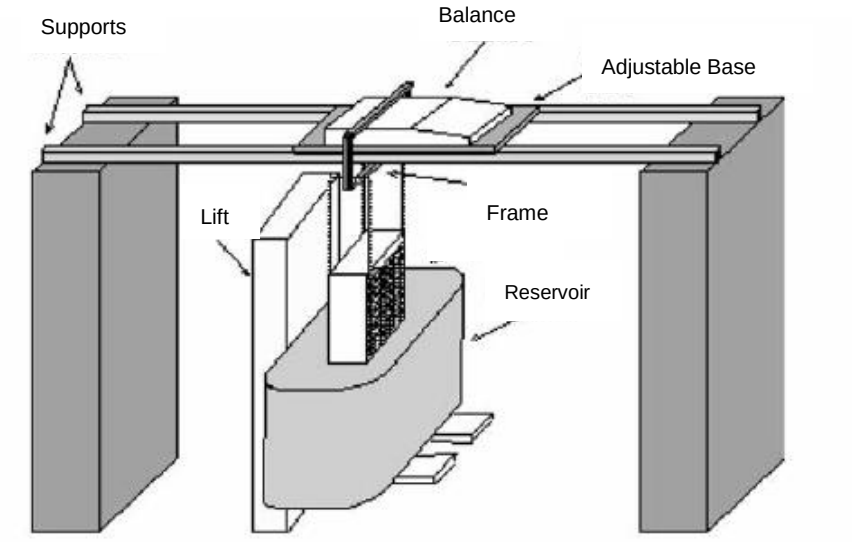

Figure 3.5 (b) An alternative apparatus for carrying out dynamic dip tests.[99]

There are two main types of apparatus used to carry out dip tests. The first (illustrated in Figure 3.5 (a)) consists of a large water reservoir, a smaller submerged air reservoir to control the submersion of coils by displacement of water using compressed air and a structure to suspend and weigh the heat exchanger. In order to initialize a test, the air vent is closed,

and the air supply then fills the displacement tank, causing the water level to rise and submerge the test specimen. Once the specimen is submerged, the air supply is closed. The water in the tank is agitated and a fine brush is used to remove bubbles from the heat exchanger surface. To monitor the drainage, the air vent is suddenly opened to allow water into the displacement tank so that the water level in the main reservoir drops.

In the second type (see Figure 3.5 (b)) it is the entire reservoir which is raised to submerge the exchanger rather than raising the water level in a fixed reservoir. This second method is much simpler and was used in this work. In these measurements the exchanger was suspended on a balance using a wood frame. The balance used can measure maximum 3000 g and uncertain less than 0.01 g. An adjustable lift carried the water reservoir which sat below the exchanger which contained sufficient water (20 litres) to immerse it. In the experiment firstly the refrigerant inlet and outlet of the heat exchanger were sealed. The balance was then zeroed and the reservoir moved up to immerse the heat exchanger. The water in the reservoir was agitated to remove air trapped on the air-side heat transfer surfaces. The reservoir was then lowered. When the water level reached the bottom of the heat exchanger, the mass was recorded at 5 s intervals for 90 s and then at 30 s intervals for an additional 240 s.

Three heat exchangers were tested to allow comparison. The contact angles shown in the Table 3.1 were recorded for small pieces of aluminium cut from the heat exchangers. These samples were not ideal for contact angle measurements because they had a pattern embossed into them which can only be partly removed by pressing them flat. This means that probe droplets tended to roll off from the most hydrophobic areas and only those which pinned at less hydrophobic region could be measured. Hence the

apparent contact angle reported in the Table 3.1 is less than 150^{o}. However, most of the surface was clearly superhydrophobic since the droplets rolled at tilt angles of a few degrees.

Table 3.1 The apparent contact angles of samples of aluminium heat exchanger treated with various coatings.

Specimen	Contact Angle	Coating Method
1	44°	Untreated aluminium
2	136°	Zincated evaporator treated with HDFT
3	5°	Zincated evaporator treated with 6-mercapto-1 hexanol

3.2.2 Results and Discussion

In the first experiment the heat exchangers were suspend from the balance vertically as shown in Figure 3.6.

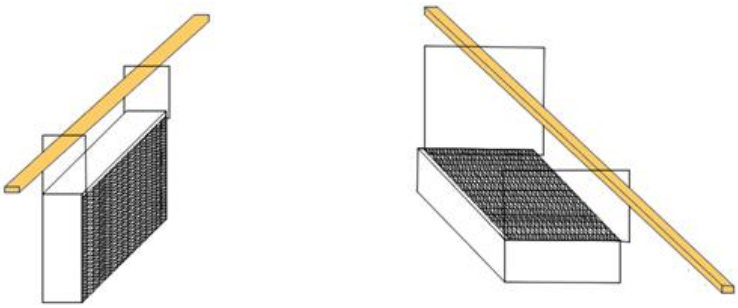

Figure 3.6 Illustration of heat exchangers mounted vertically (left) and horizontally (right) for dip testing.

Dynamic dip test results in the form of mass as a function of time are shown in Figure 3.7 for three specimens in a vertical orientation. The lines show a monotonic decrease in the mass of retained water for all heat exchangers. All three heat exchangers initially hold a similar amount of water and all show dramatic water loss during the first 30 s, followed by

slower loss. After 340 s the final retained mass was established. The superhydrophilic coated evaporator gave similar performance to the bare heat exchanger, although close examination showed that the superhydrophilic exchanger did lose slightly more water throughout the experiment and retained slightly less water at the end. This is what would be expected from the literature. Conversely, and contrary to expectations, the superhydrophobic coated heat exchanger showed less efficient water loss than the bare heat exchanger. The mass does drop more rapidly during the first 20 s of the experiment but the final amount of retained water is significantly larger than for the uncoated or the superhydrophilic cases.

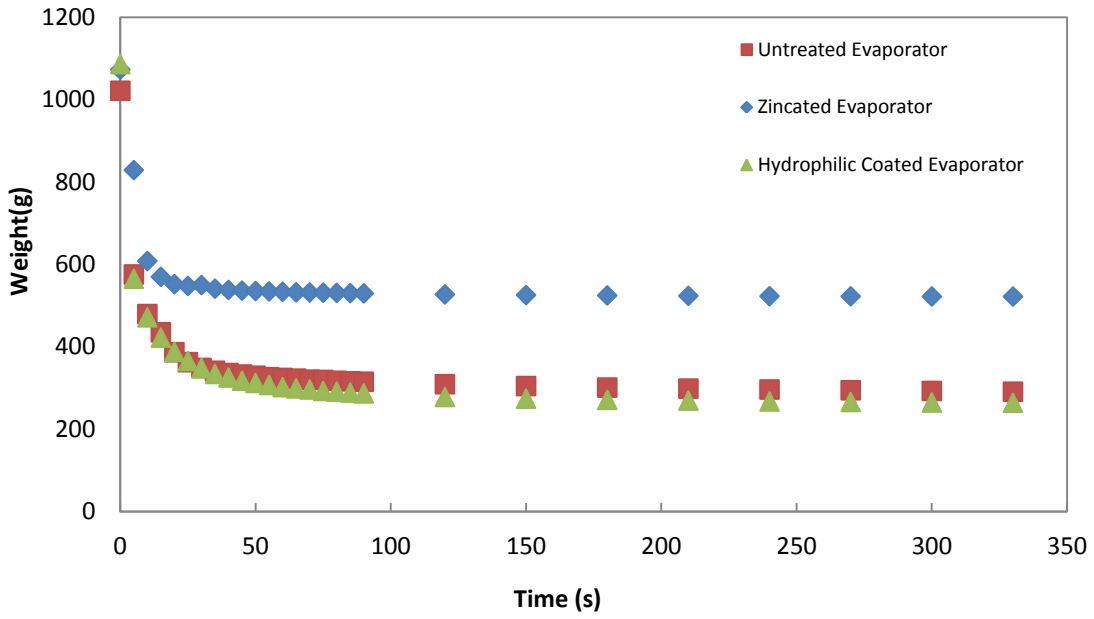

Figure 3.7 Results of dip tests on three different vertically mounted exchangers showing the mass of the retained water after removal from bulk water.

These unexpected results arise from the water drainage mechanism of louvered fin heat exchanger. For the louvered fin heat exchanger, water sitting between the fins can drain through the louvers and discharge at the bottom of the exchanger. This mechanism can also occur on the superhydrophilic coated heat exchangers. However, with the

superhydrophobic coated heat exchanger the water is forced into the space between the fins when the heat exchanger is immersed in the reservoir but the drainage fails because it depends in the water escaping through small gaps. It is well known that it is difficult to force water through any orifice that has a very high contact angle due to the effect of the surface tension, which resists the changes in geometry. A simple illustration of this effect is shown in Figure 3.8 which shows a tea strainer which was given a superhydrophobic coating using a similar process to the heat exchanger (copper electro plating then electroless silver deposition). With this coated tea strainer water is prevented draining from the mesh, even though it is clearly completely porous so it can hold water despite its open woven metal structure.

Figure 3.8 superhydrophobic coated tea strainer

For the superhydrophobic heat exchanger, the louver gaps on the fins are similar to the gaps in the tea strainer in that they allow ready access by liquid water when they are uncoated but they prevent water penetration when they are superhydrophobic, which causes water to be trapped so it cannot escape even after extended drainage time. This effect has not been observed previously with superhydrophobic exchangers but Liu *et al.* have

published a study where they investigated effects of making louver fin heat exchangers hydrophobic (up to 110°) and hydrophilic (30°). They found that the water retention did not depend only on the wettability, it also depended on the on the heat exchanger geometry. In particular, reduced wettability of a heat exchanger did not always reduce retention in a dip test; retention was reduced in simple planar exchangers but not with compact systems. Conversely, in a flat-tube louvered design the effect of surface wetting ability becomes relatively more important because the drainage path is more tortuous so increased wetting in hydrophilic heat exchangers helps to reduce water retention.[100]

To separate out the effect of hydrophobicity from the trapping effect described above, the dip tests were repeated with the heat exchanger suspended horizontally rather than vertically, to ensure the water inside heat exchanger drained by dropping through fins instead of by bottom discharge (Figure 3.7). The remaining aspects of the experiment were kept the same.

The results (Figure 3.9) showed completely different trends compared with the first experiment using vertically mounted heat exchangers.

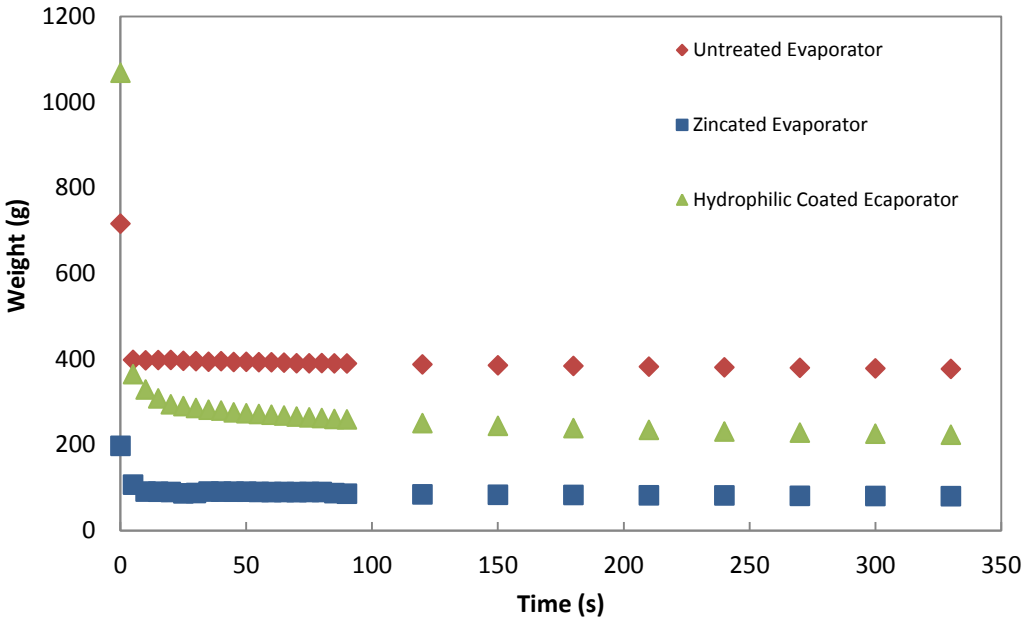

Figure 3.9 Results of dip tests on three different horizontally mounted exchangers showing the mass of the retained water after removal from bulk water.

In this geometry all the exchangers drained much more quickly than in the vertical orientation. However, it is very clear than the uncoated exchanger shows the largest water retention and indeed the amount of retained water is actually slightly higher than that with the vertical orientation. In contrast the superhydrophobic coated heat exchanger shows a slight improvement in the retained water but the main difference is the time taken to reach the stable value. The most dramatic change is in the superhydrophobic coated exchanger which shows a very large improvement in the retained water, falling to the lowest value by a considerable margin. The difference in the mass of retained water changed from ca. 520 g to ca. 80 g on changing the orientation. This is very clear evidence that the geometry of the exchanger does have a huge effect on its water retention of superhydrophobic systems. The effect is much less noticeable with uncoated or superhydrophilic exchangers so has not attracted much

attention while this is the first time that it has been possible to measure superhydrophobic exchangers and therefore see the extent of the effect.

3.3 Surface Stability

Stability and durability are a major concern in many engineering applications of superhydrophobic/superhydrophilic surfaces. In previous experiments on superhydrophobic zincated alumiuium carried out at QUB the surfaces showed no signs of degradation over the timescale of the experiments although if they were left exposed to the atmosphere for weeks or months, a white layer, believed to be zinc oxide, formed on the surface. However, in initial experiments on the coated heat exchangers prepared during this study the degradation was much more noticeable and a white deposit was found on the surface of coated pieces after just one experimental run. Initially this was assumed to be due to the coating being poor quality, which could be improved by using the protocol discussed above, however, even with the optimized procedure the problem persisted. Indeed the effect could also be observed for samples of flat aluminium where rinsing problem etc do not arise. Figure 3.7 compares the properties of the flat superhydrophobic Cu and Al prepared by zincation and/or electroless deposition of silver followed by treatment with HDFT in the normal way. Two specimens were immersed in water for 24 hours and any changes were observed.

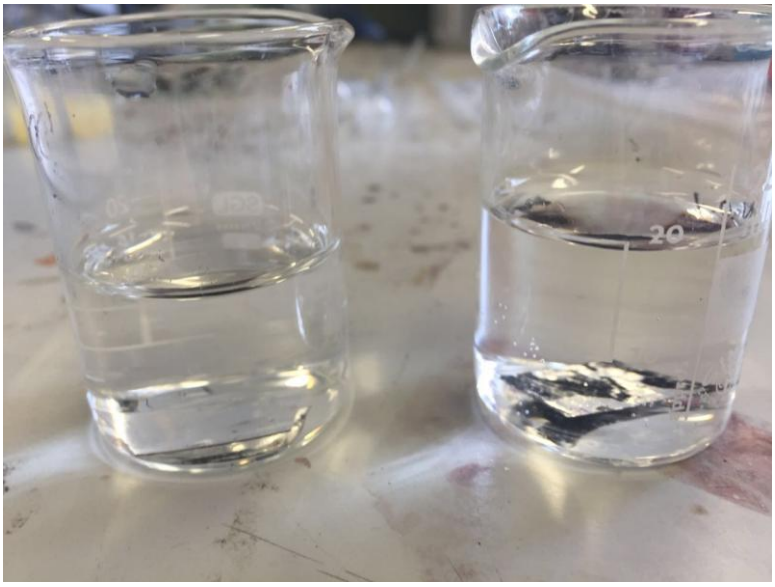

Figure 3.10 (a) Copper and aluminium samples coated as described in the text and immersed in water immediately after coating.

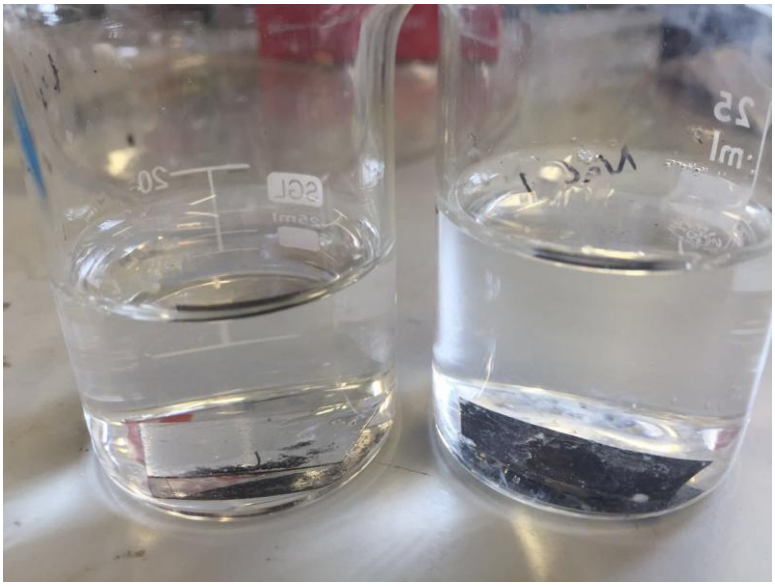

Figure 3.10 (b) The same copper and aluminium samples after being submerged in water for 24 hours.

Initially, a ‘silver mirror’ was observed for both coated pieces when they were submerged and viewed at a glancing angle, as shown in Figure 3.10 (a). In this experiment, the copper and aluminium plates were different

thickness and the copper plate was flatter than aluminium plate so it gave a better reflective ‘silver mirror’. The presence of a ‘silver mirror’ is due to the formation of an interfacial layer of air between metal surfaces and bulk water which indicates that the metal surface is superhydrophobic. Figure 3.10 (b) shows the same plates after immersion for 24 hours where it is clear that ‘silver mirror’ effect no longer appears on the coated aluminium sample, which also had a white deposit on the surface. Compared with aluminium, the copper surface still showed a good reflective silver mirror after dipping in water for 24 hours. One possible reason for the loss of the silver mirror might be that the water pressure at the bottom of the beaker was sufficient to force water into the surface texture, displacing the air. This is a well-known effect with conventional superhydrophobic coatings that repel liquids by trapping air inside microscopic surface pockets, these typically lose their properties when liquids are forced into those pockets and the air layer is displaced. However, with these conventional systems, provided the surface coating is not damaged, their superhydrophobicity can be restored by drying the surface. Unfortunately, in the current work when the aluminium piece was dried and then tested again in water the surface completely wetted, showing that the sample was not flooded but was in fact destroyed. This is consistent with the appearance of a white decomposition product on the surface. The most obvious explanation for this is that the surface may have corroded as the result of a non-continuous silver layer being deposited onto the acid-etched zinc surface, allowing water access to any residual zinc left after the electroless deposition step.[101]

In order to identify the composition of white deposit, the sample was then analyzed through Scanning Electron Microscopy (SEM) and Energy Dispersive X-Ray Analysis (EDX) which gave the distribution of elements in

the samples. Freshly prepared zincated-Ag-HDFT aluminium sample was also analyzed for comparison. SEM/EDX maps of the elements present are shown in Figure 3.11. Although a number of elements were found in both fresh treated and tested aluminium pieces, the percentage of aluminium, oxide and zinc are the most important. The EDX analysis in Figure 3.11 (a) of the freshly treated coated sample shows the atomic composition was Al 70.8 %, Zn 7.9 %, Ag 7.2 % and O 12.3 %, suggesting that some oxidation happened even in the one day between preparing and analyzing the sample. The sample which was immersed in water for 24 hours had Al 30.8 %, Zn 1.2 % and O 62.4 %.

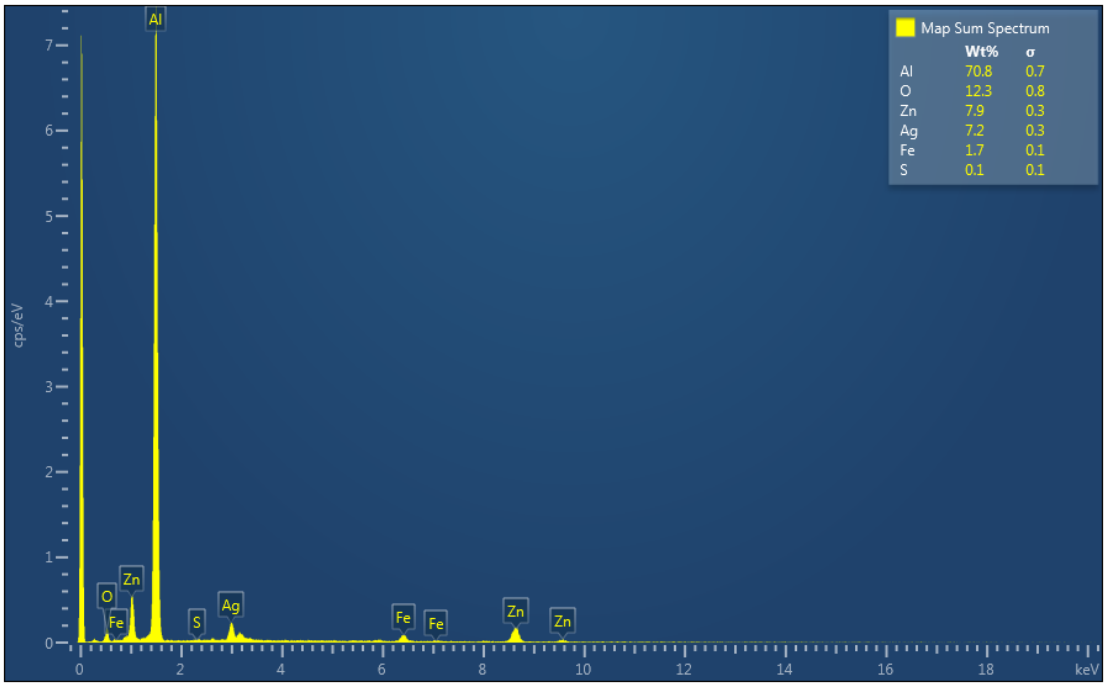

Figure 3.11 (a) EDX spectrum of fresh superhydrophobic treated aluminium specimen.

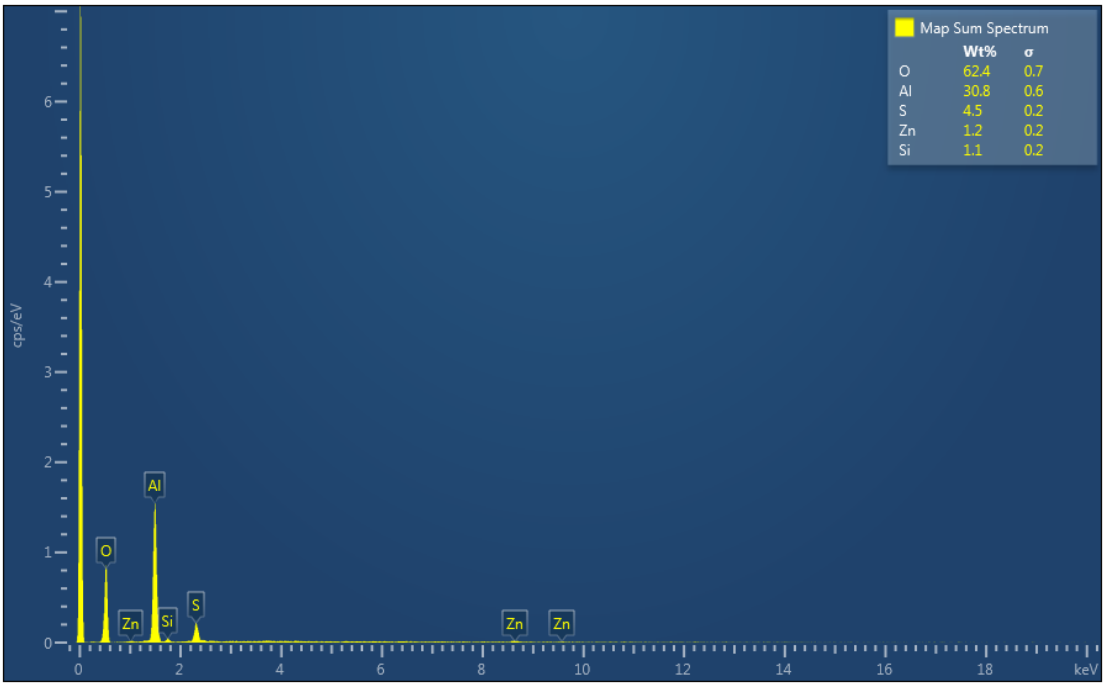

Figure 3.11 (b) EDX spectrum of degraded superhydrophobic treated aluminium specimen.

The most obvious reason for the increase in oxygen content would be that the most easily oxidized component of the coating, the residual metallic zinc, has been further oxidized and the coating was a Zn oxide or hydroxide layer formed as shown below.

$$2\,Zn + H_2O \rightarrow ZnO + 2\,H^+$$

$$2\,Zn + 2\,H_2O + O_2 \rightarrow 2\,Zn(OH)_2$$

However, the dramatic reduction in the zinc content of the deposit on the surface shows that it is not a zinc salt but is aluminium oxide. Indeed it is well known that aluminium can be protected from oxidation by placing metallic zinc in contact with it as a sacrificial anode. Here the zinc presumably also acts as a sacrificial anode but the oxide layer which is formed is not well attached and falls off, a process that can continue until the zinc is completely oxidized and the aluminium starts to be oxidized in its

place. This shedding of the surface textured layer would also explain the complete loss of silver from the sample after 24 hours immersion since it would be shed along with the zinc oxide layer.

3.4 Specimens Under Moist Conditions

The next step was to test for corrosion effects under the operation conditions of a conventional heat exchanger. A total of 8 specimens which were pieces cut from evaporators with different surface coatings and contact angles were tested in this experiment. These were divided into 4 pairs, one sample which was treated with HDFT and one which was coated with 6-mercapto-1-hexanol, these later samples were superhydrophilic.

The specimens in first pair were stuck onto the working surface of the heat exchanger as it operated in the cooling system. The second pair was stuck onto a different part of the heat exchanger which was not contacted by the hot moist air. Specimens in this group were therefore cooled but sat in the ambient temperature and humidity (around 21 °C and 50 %). The two specimens in third group were fixed inside the tube which connected the mixing chamber to the heat exchanger. These two specimens were in contact with moist air but were not cooled. Specimens in group four were placed in ambient environment as a control. The chiller was turned on which reduced the coolant temperature from 19.5 °C to 4.5 °C in the first ten minutes and continuously operated in the range of 4.5 °C to 8.9 °C for a total of an hour. During the experimental runs the heat gun worked every twenty minutes to heat the air followed by 5 minutes breaks to refill the steam generator, as described above. Contact angles were measured after each test and compared with initial data. The relative humidity of the input air was

tested at 4 different values in the range 30 % to 69 %. The results are listed in Table 3.2 and Table 3.3. The uncoated aluminium metal has a contact angle of 44°.

Table 3.2 Contact angles of hydrophobic Al pieces in the experiment under different conditions.

	Contact Angle		
Relative Humidity	**Specimen was cooled under moist hot air**	**Specimen was cooled**	**Specimen was under moist hot air**
Before test	131°	128°	136°
31 % - 34 %	125°	127°	134°
41 % - 44 %	114°	114°	130°
51 % - 54 %	102°	109°	131°
61 % - 64 %	104°	110°	133°

Table 3.3 Contact angles of hydrophilic Al pieces in the experiment under different conditions.

	Contact Angle		
Relative Humidity	**Specimen was cooled under moist hot air**	**Specimen was cooled**	**Specimen was under moist hot air**
Before test	4°	6°	5°
31 % - 34 %	13°	9°	8°
41 % - 44 %	15°	10°	12°
51 % - 54 %	15°	22°	15°
61 % - 64 %	22°	19°	15°

It can be seen from the table above that the superhydrophobic coated aluminium pieces contacted with moist air showed some degradation when the relative humidity of the input air was 34 %. The degradation was not uniform so here an average value taken from 3 points is given. When the humidity of the input air increased, the reduction of contact angle became larger until at 61 - 64 %

the final contact angle after only 1 hour under normal operating conditions was just 104°. These data suggest that it is either the heating and/or the condensation of moisture which caused the degradation. However, the experiments where the samples were placed in the input air stream but allowed to reach thermal equilibrium showed very little degradation over the time course of the experiment. Conversely, samples which were stuck onto cold surface and therefore had some water condense onto them since they were open to the atmosphere and at a temperature below the dew point also showed some degradation but to smaller extent than the samples which were both cooled and exposed to warm wet air. This clearly demonstrates that it is the condensed water rather than the increased temperature that leads to degradation of the superhydrophobic surfaces.

When the experiments were repeated with the superhydrophilic samples similar trends were observed. The largest change in contact angle was with condensation from warm wet input air. However, the contact angle changes were small compared with the hydrophobic coated metal, presumably because the degradation creates a surface that is hydrophilic in any case, so the change from superhydrophilic to hydrophilic is smaller than the change from a superhydrophobic surface which results in the same final product.

3.5 Superhydrophobic Treated Copper Powder

The low stability of the zincated surface meant that it was necessary to develop an alternative method for coating the heat exchangers to make them both superhydrophobic and stable. The method chosen was an extension of an earlier method where copper powder was treated to make it superhydrophobic and then fixed to the surface using a layer of 3M DisplayMount™ adhesive.

To prepare the superhydrophobic powder, copper powder (14 - 25 μm, Goodrich Ltd.) was washed with nitric acid (0.05 %), washed with distilled water and immersed in silver nitrite solution (0.1 M) for 1 minute and shaken. The silvered copper powder was filtered and washed with distilled water before being dried in an oven overnight. The dried powder was then treated with HDFT solution in DCM (1 mM) for 24 hours before being filtered and washed with DCM and left to dry. The superhydrophobic copper powder was applied to the heat exchanger by first spraying a layer of high strength adhesive which was then diluted *in situ* by brushing on toluene which is ran between the louvered fins. The system was then allowed to sit for 2 - 3 minutes until the surface was tacky at which point the superhydrophobic powder was sieved onto the exchanger. The excess powder was first shaken off and then blown off by compressed nitrogen.

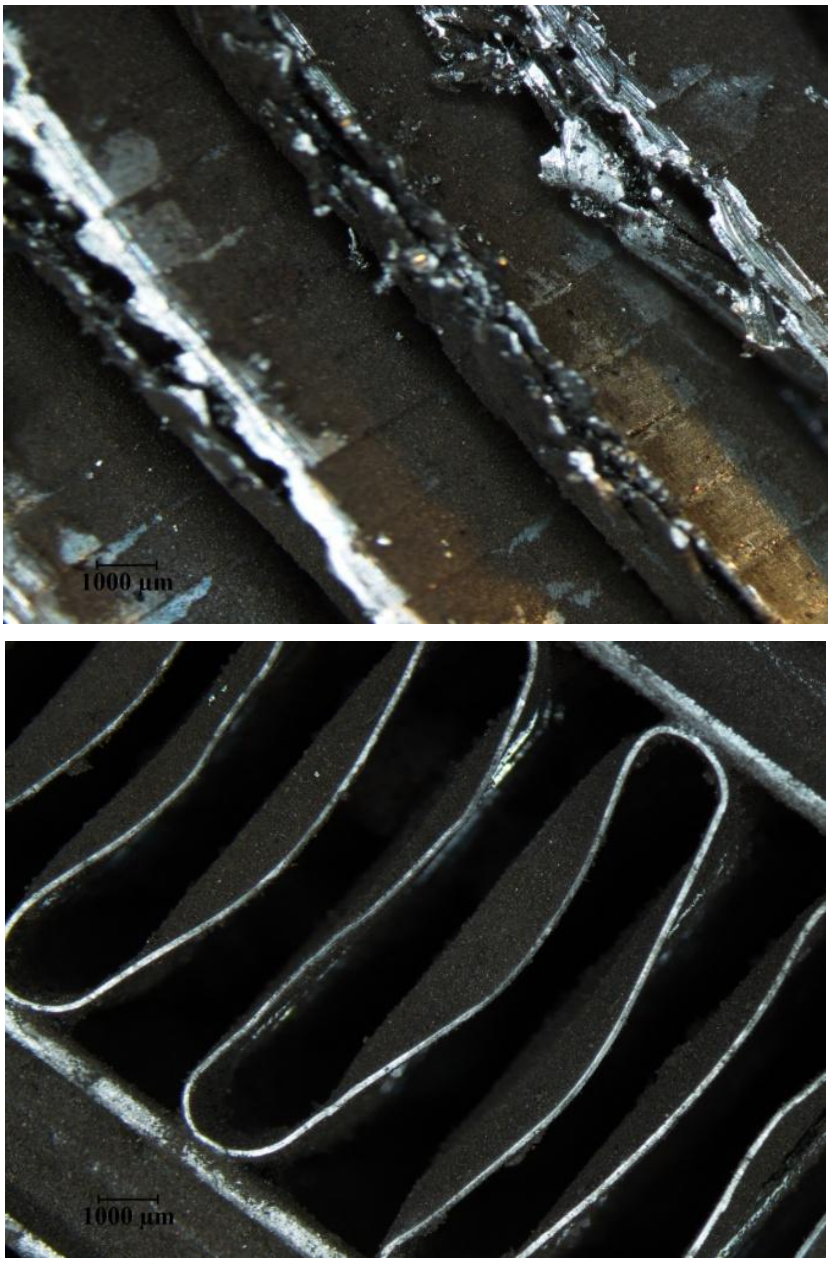

Figure 3.12 Images of the powder coated surface obtained using a low power microscope.

The external surface of the coated heat exchanger appeared to have a uniform thin coating of copper powder but a sample of the exchanger was cut open to also allow the inner surface to be inspected, since it would be expected that any problems with the coating would be on the inner surfaces. The coated surfaces were imaged by a Nikon SMZ800 stereomicroscope and are shown in Figure 3.12. The images in the Figure 3.12 display clearly

that the aluminium surfaces which were inspected were covered with copper powder evenly so the performance of superhydrophobic copper powder coated evaporators was then tested.

Dynamic Dip Test

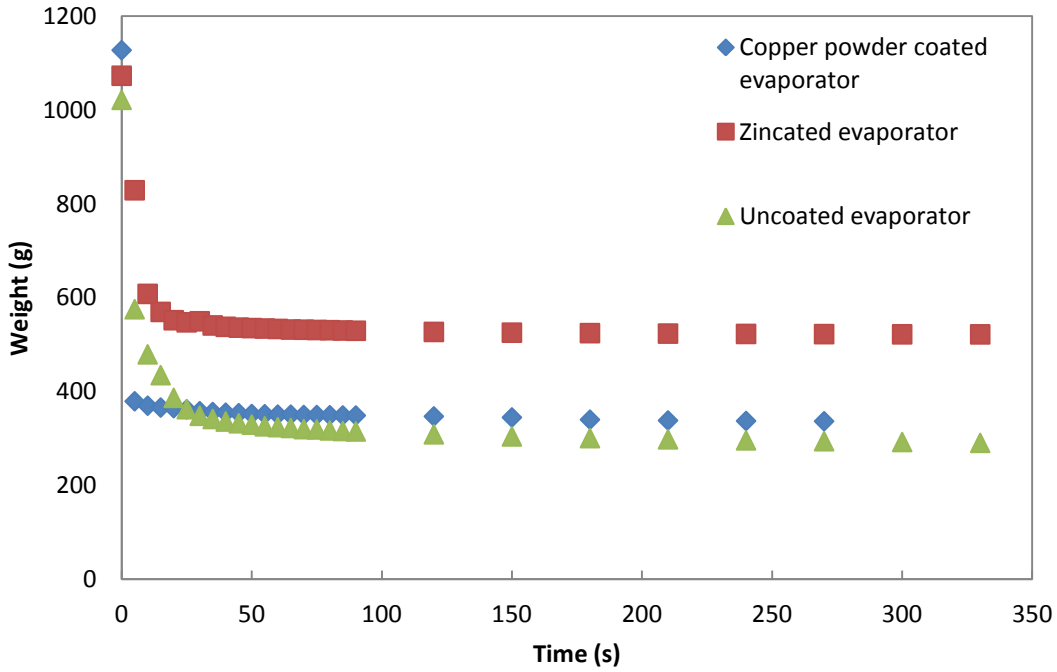

Figure 3.13 Results of dip tests on three different vertically mounted exchangers showing the mass of the exchangers plotted as a function of time after removal from water.

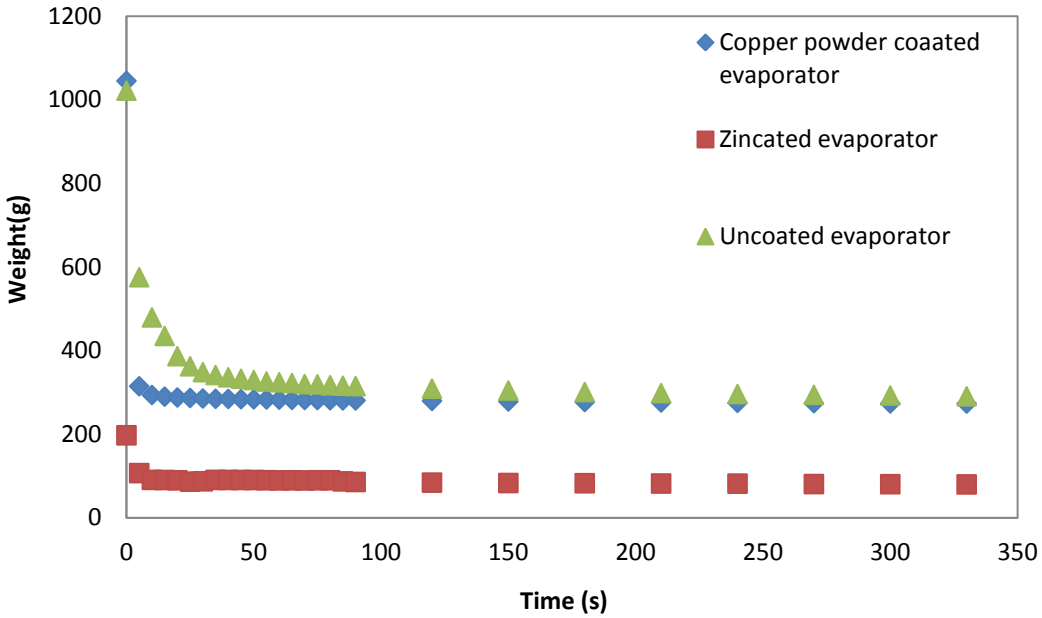

Figure 3.14 Results of dip tests on three different horizontally mounted exchangers showing the mass of the exchangers plotted as a function of time after removal from water.

The dynamic dip tests which were described above for zincated superhydrophobic coated exchangers were repeated for the Cu powder coated exchangers. The results of these dip tests for both vertically and horizontally mounted heat exchanger are shown in Figure 3.13/3.14 which compares the results from both types of superhydrophobic exchangers with a simple uncoated control. The results show that for the vertical orientation the zincated exchanger retained significantly more water than the copper powder one. However, neither of the superhydrophobic exchangers drained as well as the simple control. For the zincated sample this was due to the coating preventing drainage though narrow channels in the exchanger. This effect also seemed to occur for the copper powder coated systems. When the heat exchangers were hung horizontally, the results showed a different trend, where the zincated heat exchanger held much less water at the beginning and retained less water at the steady state than either the uncoated or copper powder coated exchangers. In this case the horizontal

geometry takes advantage of the fact that the superhydrophobic coating allows the water to drain away through the open channels. The fact that the copper powder coated heat exchanger shows less efficient drainage in the horizontal suggest that the coating is either less hydrophobic than the zincated one or that the coating may be partly blocking the open channels and preventing water loss.

Imaging the Internal Structure of the Heat Exchangers

The obvious way to check whether the coating blocks the channels in the exchanger would be to cut the exchanger open and look directly at the internal structure. Unfortunately, the exchangers are quite fragile and it is difficult to cut them open without damaging the structure. As an alternative, a system was built which allowed the shadows of the fins within the exchanger to be observed. A photograph of the experiment set up is given in Figure 3.15. A strong and nearly parallel light source (ZEISS IKON® Halogenlampe (24V/150W) 35 mm slide projector) was placed at the front of tested evaporator. A paper was attached on the back side of evaporator to act as a screen which showed the shadow of the interior structure.

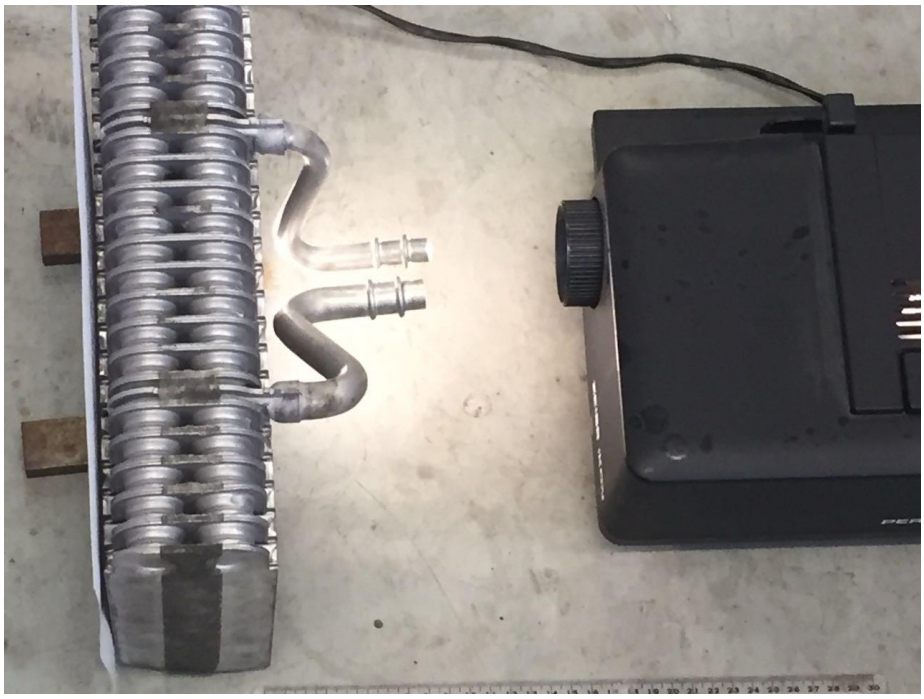

Figure 3.15 Photograph of the system used to inspect the interior of the exchangers.

An uncoated evaporator, zincated evaporator and copper powder coated evaporator were tested and photographed, with the results shown in Figure 3.16 (a - c). The images showed clear differences between the coated evaporators and the uncoated one. The shadow of the uncoated evaporator showed the expected structure, while in the image from the zincated evaporator there are some additional small shadows on the fins which could be due to small areas of oxidation after coating. Conversely, parts of the air side of copper powder coated heat exchanger shadow showed obvious signs that some of the channels were blocked by glue and copper powder. This was probably due to uneven application of the adhesive during the during the glue spraying step causing uneven copper powder coating on the surface. These blockages would be expected to strongly affect the air path and cause a significant pressure drop compared to more open uncoated exchangers.

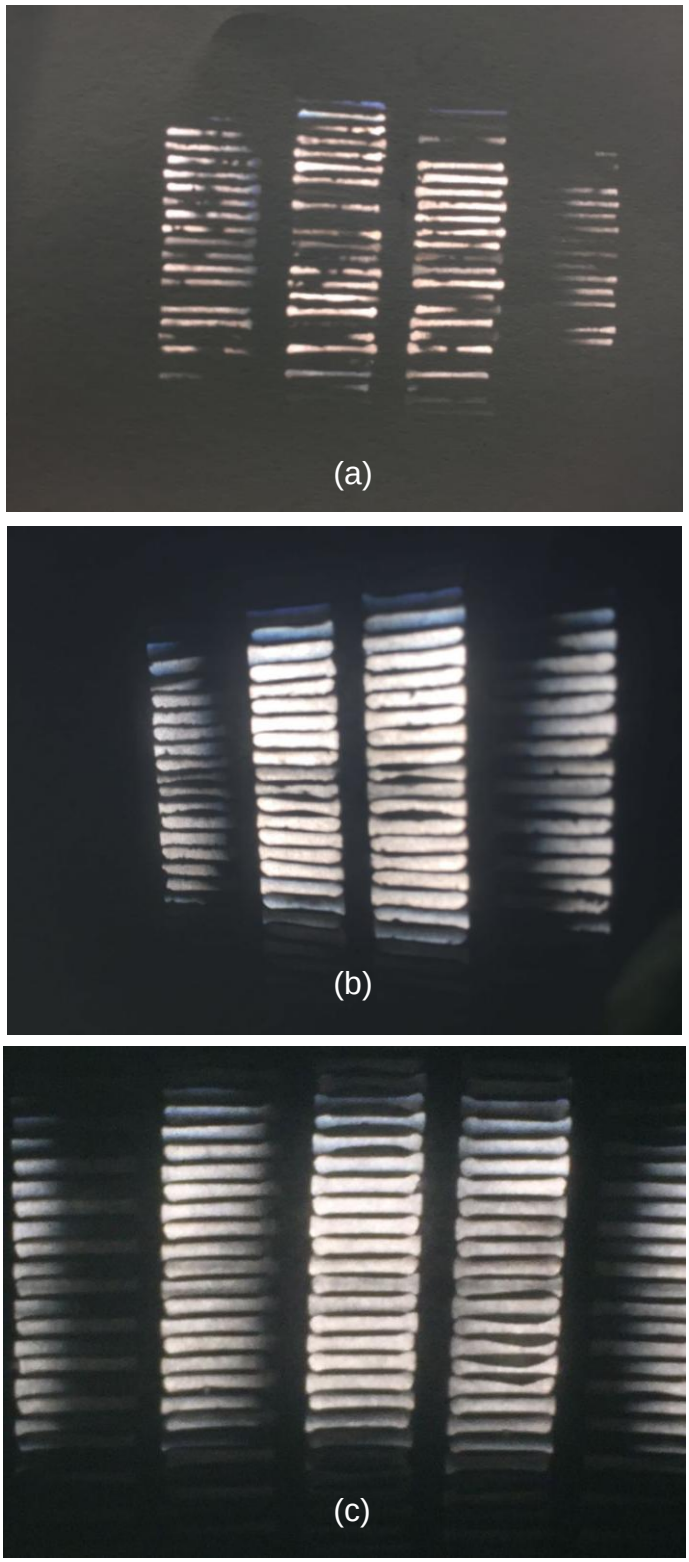

Figure 3.16 (a) Photograph of the shadow of copper powder coated evaporator. (b) Photograph of the shadow of zincated evaporator. (c) Photograph of the shadow of uncoated evaporator.

In addition to simple blockage, Yuan *et al* have shown that channels with a larger surface roughness tend to have higher pressure drops at a given mass flow rate.[102] This means that the effect of roughness cannot be ignored in microchannels, so that even for the zincated coated heat exchanger where there is no simple blockage, the grainy oxides will increase the surface roughness and this may therefore also lead to an air velocity decrease compared to smooth uncoated exchangers. Of course this means that for the copper powder coated heat exchanger, the blockage of fins caused by glue and powder and increased surface roughness may both contribute to the total observed air velocity difference.

3.6 Measurements of the Performance of Heat Exchangers

3.6.1 Pressure Drop (Air velocity difference)

As discussed above, the pressure drop could not be measured directly so the outlet air velocity was measured as a way of indicating the relative friction factors of the various exchangers. In the experiment, the flow rate through the system was fixed. Inlet air velocity was recorded at the beginning of experiment, and outlet air velocity was taken over a period of 15 minutes. The experimental results are shown in Figure 3.17 - 3.20, where the outlet air velocity is plotted against operating time. Heat exchangers with different coating methods were compared to analyze the effect of coating surface on air-side performance.

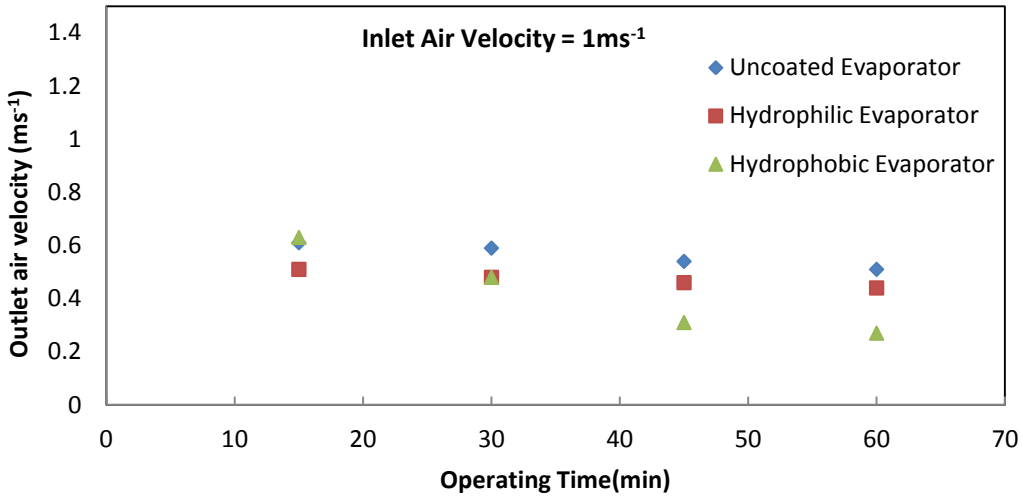

Figure 3.17 Outlet air velocity of vertical heat exchangers at 1 m s^{-1}.

Figure 3.17 shows the outlet air velocity of heat exchangers at the same inlet air velocity when the heat exchangers were mounted vertically in the testing system. The results show that all heat exchangers had a decreased outlet air velocity with operating time. The main reason for the phenomenon is that the condensation accumulates on the surface with time. The heat exchangers were operated under wet condition as discussed above, which means the temperature of the surface of the heat exchangers is below the dew point of the input air. With humid and moist air flowing though the cold surface, condensation occurred and the condensed water was retained on the fin surface and blocked the air side flow path. The outlet velocity of air did tend towards a stable value over time for all heat exchangers. The reason for the value reaching stable value was that the droplets collect, reach their maximum size and shed from the surface because of air flow force or gravity. At the beginning of the run the condensation accumulates on the heat exchanger surfaces but eventually a balance between the rate of condensate deposition and the rate of droplet shedding is achieved. The

equilibrium value will depend strongly on the experimental conditions because, for example, shedding of droplets that bridge between the fins in a fin-tube exchanger will depend on the local air velocity, the quantity of condensate in the tube wake region and the roll off angles.[103]

The outlet air velocity of the uncoated heat exchanger is higher than the two coated heat exchangers. There is a small decrease of the outlet air velocity during the operation which is around 16 % after one hour. This is consistent with the observation that the retention performance of uncoated evaporator as shown in the dynamic dip test is good. Again this probably to be expected since the system was designed to be used in a vertical orientation and without a hydrophobic coating.

The results also shows that the outlet air velocity of superhydrophilic coated heat exchanger is slower than the uncoated heat exchanger but that it only changed slightly during the operating time. The lower outlet air velocity at the beginning could be explained by the increased roughness due to the coating causing increasing friction, as discussed above. Although of course the coating does have a finite thickness which would also impede the air flow. However, since the coating is only ~ 5μm thick,[101] this effect would be expected to be small. More interestingly, the outlet velocity dropped by a smaller amount for the hydrophilic system than the uncoated control (13 % vs 16 %). This is consistent with the observation that the hydrophilic heat exchanger showed better drainage performance in the dip tests. The main reason for this improved performance is that droplets on the hydrophilic fins surface were flatter and lower volume than those on the superhydrophobic coated and uncoated heat exchangers. This is an example of the general observation that if the same area of the heat exchanger is covered by condensate, the mass of retained condensate will decrease as the

wettability increases. In addition, no condensation bridges were observed on the hydrophilic coated heat exchangers since the ability of droplets to interact between adjacent fins surfaces was lowered in the superhydrophilic systems. These results are in agreement with those of Liu[87] who noted that hydrophilic treatment consistently helps reduce core pressure drop across the heat exchanger, especially for high fin density. Liu also found that heat exchangers with lower contact angles retained much less water than hydrophobic ones in wind tunnel tests.

The data in the Figure 3.20 also show that the result given by the superhydrophobic evaporator was not as good had been hoped when the project was planned. Although the initial difference between inlet and outlet air velocities was similar to that for the other exchangers, the final value was found to be much larger (57 %) than those for uncoated (16 %) and superhydrophilic (13 %) evaporators. The large slope of the air velocity change with time followed the same trend as the dynamic dip tests which indicated the superhydrophobic heat exchanger had higher retention than the other exchangers. As discussed above, the design of the exchangers meant that water could trapped between the louvered fins and could not drain away because its high surface tension prevented drainage through the drainage holes. In addition, condensate bridging which occurs when condensate on one fin surface begins to interact with condensate on the adjacent fin surface (see Figure 3.24) was observed, due to the narrow fin spacing. This phenomenon is related to surface wettability which determined the height of the droplet adhering to the fin surface and so is expected to be larger on more hydrophillic surfaces, as shown in Figure 3.25.

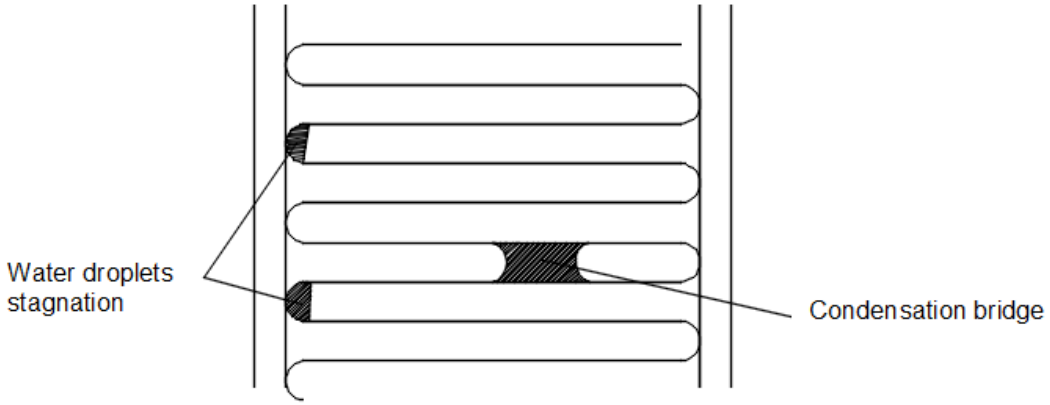

Figure 3.18 Schematic of a condensation bridge.

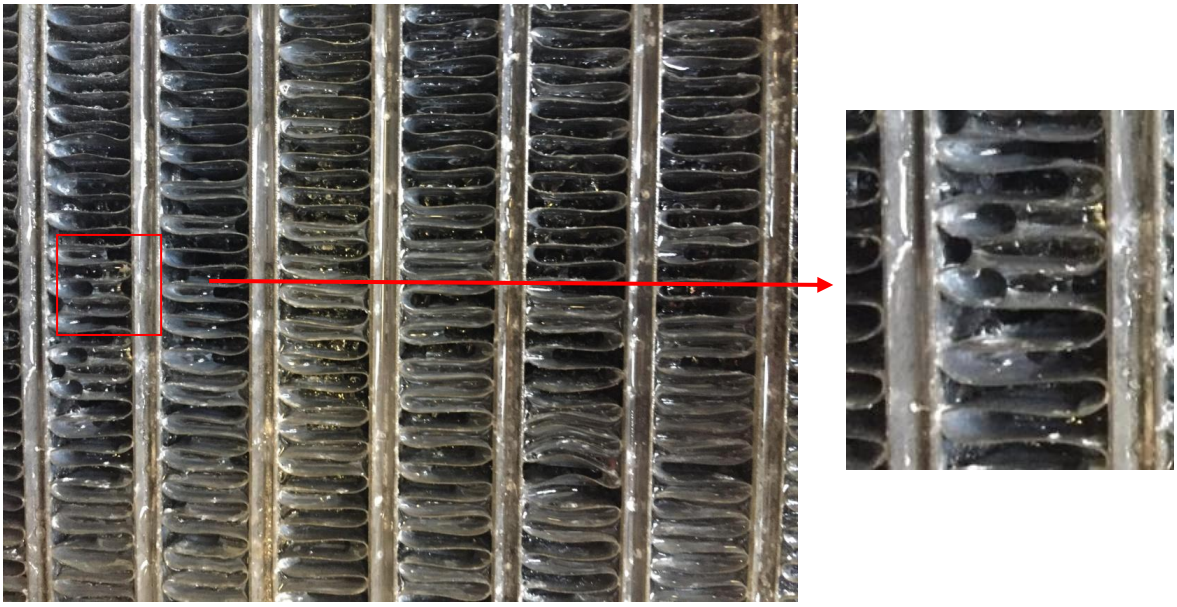

Figure 3.19 Condensation bridges formed between hydrophobic fins in the experiment.

The results of dynamic dip tests did suggest that while the performance of the superhydrophobic heat exchangers was compromised by the design when the system was suspended vertically. This was not the case when it was fixed horizontally, so the air velocity measurements were also carried out with the exchangers held horizontally, giving the data shown in Fig. 3.26.

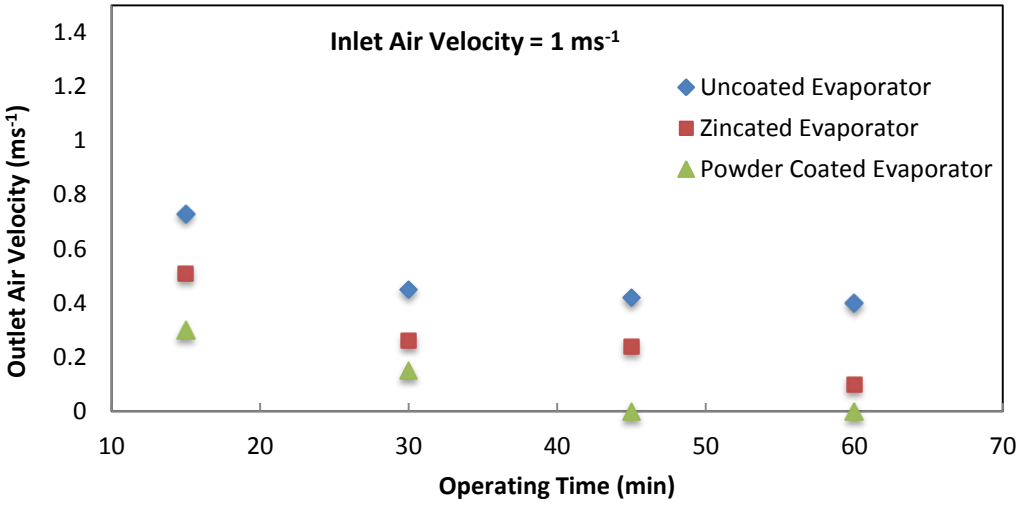

(a)

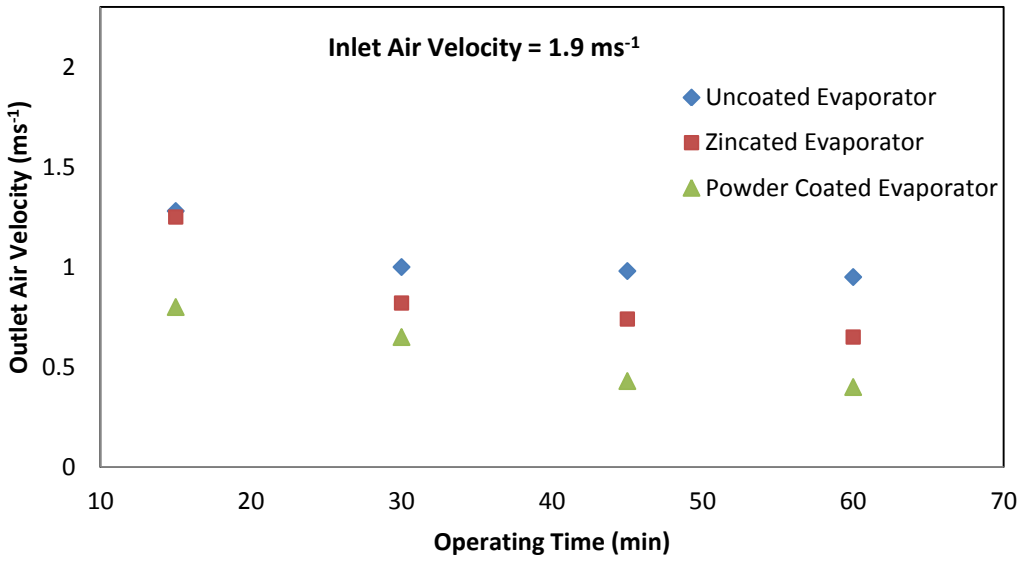

(b)

Figure 3.20 Outlet air velocity of horizontal exchangers at 2 different inlet air velocities. (a) 1 m s^{-1} and (b) 1.9 m s^{-1}.

For the uncoated evaporator mounted horizontally, the air velocity falls much more dramatically with time than when it is fixed vertically in the system This is in accord with the dip test results and is due to the geometry of the evaporator, which is designed to be used in the vertical orientation, as

discussed above. When the air velocity is 1.9 m s^{-1}, the result is better because the higher input air velocity decreases the quantity of retained condensate by blowing droplets off to some extent.

More surprisingly, a significant drop in the output air velocity was observed over time for the zincated heat exchanger. This is contrary to the results of the dynamic dip test, where the coated exchangers showed the lowest water retention of all the systems tested, suggesting that the retention of the condensate was not simply caused by water trapping. The same effect was also observed even at 1.9 m s^{-1} where there was less trapped water but the performance was still not as good as the uncoated evaporator. Since it was shown above that the materials degrade in use it might be expected that the water retention was associated with sample degradation, since the degradation leads to loss of hydrophobicity and pinning of droplets on the surface. However, in these experiments particular care was taken to ensure that the coatings were not degraded during the short time that the measurements were made. Firstly, the exchangers were prepared in the same week that they were used and stored under dry conditions to prevent degradation, before use they were inspected to check that no white deposits were present and they were tested with water dispensed from a syringe onto various points of the surface to check that the water roll off angle was still very low. During the experiments the exchangers were only operated for approximately 1 hour and after use excess water was blown off their external and internal surfaces using compressed air before they were left to dry completely. Importantly, the exchangers were then tested again for water adhesion and it was found that even those exchangers which showed droplet pinning in use still had very low roll off angles after drying, suggesting that they had not been permanently

degraded. Figure 3.21 shows a photograph of an exchanger which had been run with coolant circulating through it for 20 minutes and it is clear that the droplets condensed on the fins are not the near-spherical droplets expected for a superhydrophobic surface but are predominantly domed with contact angles significantly less than 90 degrees.

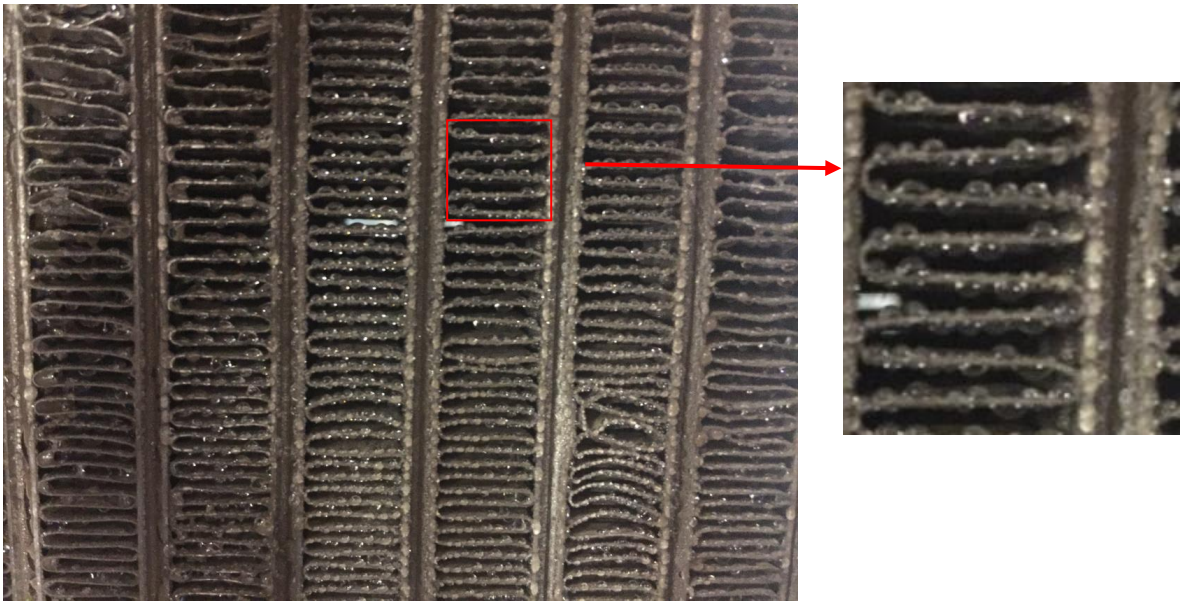

Figure 3.21 Dropwise condensates on superhydrophobic heat exchanger.

It is known that condensed droplets on even superhydrophobic surfaces can display low contact angles if the surface 'floods'. Flooding occurs when the rate of condensation is high because under those conditions the microscopic droplets which form within the surface roughness may merge with other droplets within the textured layer before they have time to escape to the surface (shown in Figure 3.22). There have been reports showing that this effect can be reduced by patterning the surface. Emre *et al.*[104] showed that by optimization the surface with rectangular array of superhydrophilic islands on the superhydrophobic surface they could reduce flooding by changing jumping-mode condensation to shedding-mode condensation.

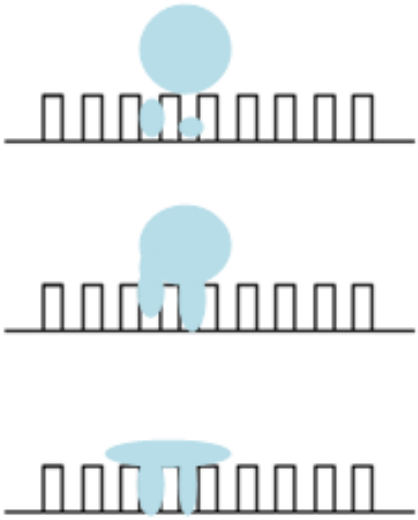

Figure 3.22 Schematic diagram of flooding on superhydrophobic surface.

In the current work it was hoped that flooding would not be a problem because previous work by John McCracken showed that for flat zincated aluminium surfaces, droplets grew larger and coalesced with neighbouring droplets before jumping from the surface to clear the condensation area under all tested condensation rates. However, flooding is dependent on the microstructure of the surface and it appears that the structure that could be achieved with the heat exchanger were just not as good as those which can be created on a flat surface. In addition, within the exchangers the fin spacing is small, so that even if the exchangers are initially covered with spherical droplets, as these grow if they are not shed they will press against the opposite surface and the pressure this creates may force the water into the texture, again give rise to flooding of the sample. Indeed, in Figure 3.21 it is clear that some of the largest trapped droplets are in the corners of the fin structure.

Tests were also carried out on the powder coated exchangers for two reasons. Firstly because the powder coating is significantly more stable than the zincated materials, so degradation should be less of a problem and secondly because the dip tests showed that the copper powder coated heat exchangers will have better drainage performance than the uncoated ones, although still not as good as the zincated materials.

The first thing to note in the results for the powder-coated exchanged is that even at the beginning of the experiment these exchangers show the largest reduction in air velocity of the three systems tested. This is due to the partial blockage of the fin structure by the adhesive/powder coating as was discussed above in section 3.7.

More surprisingly, the copper coated exchangers also showed very large increases in the air velocity drop over time, again associated with water retention. There are several possible causes of water retention. Simple coating degradation can be ruled out since these systems are known to be stable for periods of years. The next most likely cause is uneven application of the coating due to gaps in the adhesive layer or small areas where powder has not contacted the adhesive layer. Although the coatings appeared high quality when examined using optical microscopy, even small areas < 100 μm can act as nucleation centres where droplets can grow but are pinned in place. In a tube and fin exchanger such areas can have a disproportionately large effect because a blockage or partial blockage at one point along a channel affects the performance of the entire channel. In addition, although the copper powder is not expected to flood, the powder is applied as a layer so there is a real possibility of condensation occurring between the particles and droplets in that position growing until the surface is flooded, as shown in Figure 3.23.

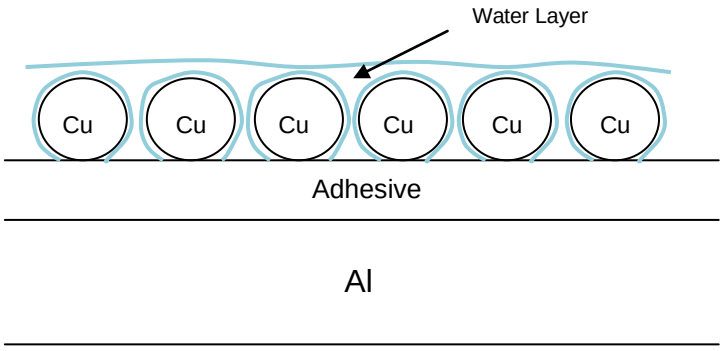

Figure 3.23 Schematic diagram of flooding on copper powder coated surface.

In conclusion, the results of the experiments show that dip tests are only a partial replacement for testing under real experimental conditions. During the dynamic dip test, condensation bridges were not found when the heat exchangers were tested in a horizontal positon while they were in the air conditioning system. This may be due to the difference between the mechanisms by which the water was added in the dynamic dip test and air conditioning experiment. In the dynamic dip test, the water is added as bulk water not droplets and sweeps away most of the water from the fin surface as it falls from the exchanger at least at earlier time. However, in the air conditioning system droplets grow on the surface and need to achieve a critical size before they are shed either under gravity or by the air flow. This means that while dynamic dip tests can give a quick assessment of the condensation performance of heat exchangers especially non-compact exchangers they cannot provide an exact retention prediction for coated, compact automotive-type heat exchangers where geometrical effects dominate the drainage process.

3.6.2 Overall Heat Transfer Measurements

The most important parameter used to characterise the performance of a

heat exchange system is the overall heat transfer coefficient, U, which measures heat transfer per unit area. In the current case the value which is measured is UA, the heat transfer conductivity, which includes the area but this can be used for comparison between the various experiments carried out since the area of heat exchanger used for cooling was fixed throughout. UA is calculated from a set of experimentally measured values for the system under test which are: the inlet and outlet air temperatures, inlet and outlet air humidity and inlet and outlet cooling water temperature. Firstly, the temperature and humidity of the input and output air as well as the mass of inlet air cooled per second is used to calculate the total amount of heat transferred, $Q_{a,}$ per second. This essentially combines the energy change associated with the heat capacity of the air with the energy change associated with changing the humidity of air during the cooling process (i.e. the latent heat of the water). The second term to be calculated is the log mean temperature difference, LMTD, which is related to the difference between the inlet air and outlet water temperature as well as the outlet air and inlet water temperature. UA is given by Q_a/LMTD.

The experimental values for 4 vertically mounted heat exchangers with different surface coatings tested under the same sets of experimental conditions are shown below. In these experiments the input air temperature was set at 33 °C and the relative humidity to 50 - 60 %, which corresponds to conditions where the exchanger is well below the dew point and significant condensation is expected. The input air velocity was varied between 1 ms^{-1} and 1.7 m s^{-1}. The temperature and humidity data were logged every second and ten seconds, respectively, during the experiment. Data where the input air was out of range (air temperature not between 32 ^{o}C to 34 ^{o}C or relative humidity beyond the range 45 % to 65 %) were removed from the calculation. Ten minutes of recorded data were averaged and used to calculate a UA value. Three experiment run under the same conditions and the average values are summarized in Table 3.4. Standard deviations were calculated for the repeat runs under the same conditions but since the number of repeats was small there were instances where the calculated values were

unrealistically small (1.5 %) and very large (21 %) for this reason the standard deviations were calculated as percentages for each of the sets of conditions and the average obtained to give a more meaningful estimate of the uncertainty in the calculated values for the UA. The average standard deviation was found to be 11 % so if the uncertainty is $\pm$ 2 standard deviation, the values the UA values are $\pm$ 22 %.

Table 3.4 Overall heat transfer conductivity for heat exchangers mounted vertically.

	Q_a (J s^{-1})[a]	LMTD[b]	Difference of Air Temperature (℃)	UA (W K^{-1})[c]
Uncoated Heat Exchanger				
V_{in} = 1 m s^{-1}	582	9.18	25.2	63
V_{in} = 1.3 m s^{-1}	744	8.66	25.9	86
V_{in} = 1.5 m s^{-1}	864	9.40	25.1	92
V_{in} = 1.7 m s^{-1}	924	5.66	24.6	163
Superhydrophilic Heat Exchanger				
V_{in} = 1 m s^{-1}	609	7.56	25.6	81
V_{in} = 1.3 m s^{-1}	790	7.12	27.1	111
V_{in} = 1.5 m s^{-1}	892	8.53	26.0	105
V_{in} = 1.7 m s^{-1}	982	7.93	25.5	124
Superhydrophobic Heat Exchanger (Zincated)				
V_{in} = 1 m s^{-1}	601	8.62	26.3	70
V_{in} = 1.7 m s^{-1}	1007	5.54	26.8	182
Copper Coated Heat Exchanger				
V_{in} = 1 m s^{-1}	614	6.17	27.5	100
V_{in} = 1.7 m s^{-1}	1022	5.37	26.9	190

[a] Overall heat transfer rate was calculated by equation (2.5) in Chapter 2.

[b] Log–mean–temperature-difference was calculated by equation (2.11). [c] Overall heat transfer conductivity was calculated by equation (2.12).

The first trend which apparent in Table 3.4 is that the overall heat transfer conductivity was found to have an obvious increase with increasing air velocity for all heat exchangers. This is due to the combination of two factors, the first is that in general the temperature difference between inlet

and output air does not depend strongly on the air velocity. This means that the heat transferred (as measured by Q_a) is larger for the higher velocities since the same cooling has been applied to a larger mass of air. Self evidently this will equate to a larger UA.

In addition, there is also a weaker trend in the values of LMTD where the LMTD is lower at higher velocities. Since the LMTD depends on the difference between the temperature of the input cooling water and the output air it essentially measures how close to the coolant temperature the exchanger has been able to reduce the air temperature. Again if the exchanger is working well the difference will be small and so will the LMTD. In the current experiments it may be that the better clearing of condensed water at higher air velocities (as shown in the pressure drop experiments) gives better heat exchange and therefore reduced LMTD. This also leads to increased UA values so the combination of both increased Q_a and reduced LMTD gives higher UA values.

Comparing the coated and uncoated heat exchangers at the same input air velocity it is noticeable that the UA values do not change very significantly. For example, the values for the uncoated and zincated exchangers are very similar to each other at both 1 m s^{-1} and 1.7 m s^{-1} input air velocities. This suggests that any dropwise condensation which has been achieved is not sufficient to change the UA dramatically. Possibly this may be because flooding of the surface leads to filmwise condensation and the potential benefits of using the superhydrophobic coating are lost. The UA values do appear to be better for the copper powder coated exchangers which suggest that they may show some dropwise condensation but the effect is really only apparent at low input air velocity. However, in assessing overall performance both the UA and pressure drop need to be taken into account. Here even small beneficial changes in UA will not be sufficient to compensate for the very large increases in pressure drop which occur with the zincated and copper powder coated exchangers. As discussed above in section 3.8.1, the output velocities are very much lower for the coated exchangers than for the uncoated systems. This means that the total amount

of air which is cooled is also much smaller, so even a small improvement in UA will not cancel out the very negative effect of the increased pressure drop on the performance of the system. This effect is not reflected directly in the UA calculated here because the calculation method used the input air velocity rather than the pressure drop when determining Q_a. More accurate calculations require a measured pressure drop which was not possible with the experimental test system available. However, even without direct measurements of the pressure drop it is clear that the superhydrophobic coated exchangers tested here do not offer any overall improvement over the normal uncoated exchangers.

In the case of the superhydrophilic coating the case is not so clear, at least at low input air velocities the coated exchanger has a marginally better UA value. This is consistent with the idea that at low velocities the uncoated exchangers have a significant amount of condensate on the surface which is not blown away by the air flow while the superhydrophilic exchangers have less condensate because the water can spread on the surface and drain away. This effect also means that the pressure drop for the superhydrophilic exchangers does not increase with time as much as for the uncoated exchangers, although the value does start lower so it does not actually fall below the value of the uncoated exchanger. This means that the performance of the superhydrophillic exchanger may be the same as that of the uncoated system or slightly better or worse, there is too much experimental uncertainty in the current measurements to be confident which case is true. These results are in agreement with the previous studies [89, 90] discussed in Chapter 1, which showed that under wet conditions hydrophilic coatings had little effect on heat transfer coefficients but gave lower pressure drops.

The exchangers were also tested in a horizontal orientation, primarily because the dip test had shown that the zincated exchangers had very low water retention in this orientation. Of course the air velocity difference measurements showed that this effect was not found when the water was condensed onto the surface rather than forced into the exchanger by

immersion. However, for completeness the UA values were measured for both zincated and copper powder coated exchangers, with the results shown below, where the uncertainty is again ± 22 %.

Table 3.5 Overall heat transfer conductivity for heat exchangers mounted horizontally.

	Qa (J s^{-1})	LMTD	Difference of Air Temperature (℃)	UA (W K^{-1})
Uncoated Heat Exchanger				
V_{in} = 1 m s^{-1}	581	6.87	25.0	85
V_{in} = 1.3 m s^{-1}	762	6.06	26.6	126
V_{in} = 1.6 m s^{-1}	852	5.04	24.8	169
V_{in} = 1.9 m s^{-1}	1098	8.44	25.4	130
Superhydrophobic Heat Exchanger (Zincated)				
V_{in} = 1 m s^{-1}	577	7.52	25.1	77
V_{in} = 1.3 m s^{-1}	780	6.40	26.5	122
V_{in} = 1.6 m s^{-1}	944	6.05	26.6	156
V_{in} = 1.9 m s^{-1}	1123	8.01	25.5	139
Copper Coated Heat Exchanger				
V_{in} = 1 m s^{-1}	591	5.39	26.2	110
V_{in} = 1.9 m s^{-1}	1202	6.85	26.9	175

In this case the results for the zincated and uncoated exchangers were almost identical at all input air velocities. The copper powder coated exchangers did give higher UA values, as was also the case for the same exchangers in the vertical orientation but again these marginal improvements will in reality be more than cancelled by the large pressure drops induced by the coating. It is interesting to note that the UA value for the copper powder coated heat exchanger did not decrease, even though it might be expected that the layer of glue and powder would have lower thermal conductivity and thus decrease the heat transfer rate. This suggest, that despite the flooding effects etc there is at least some dropwise condensation occurring to counterbalance effect of the thick glue/powder layer on heat transfer.

Chapter 4 Conclusions and Future Work

Chapter 4 Conclusions and Future Work

4.1 Conclusions

The original intention of this research work was to build on preliminary results obtained in another QUB project which appeared to show that superhydrophobic coating of heat exchangers using the electroless galvanic deposition method allowed dropwise condensation to take place and therefore should improve the performance of the exchangers. Furthermore, tests on planar substrates showed ‘droplet jumping’ and no evidence of flooding under the conditions investigated. However, the much more extensive investigations in this thesis have shown that creating these effects in an object as complex as a tube and fin heat exchanger is a much more difficult problem than was originally believed.

In this work, a method for achieving superhydrophobicity on aluminium louvered fin heat exchangers using zincation followed by electroless deposition of silver was developed. This was based on the method that had been used previously but it needed to be modified for application to the heat exchangers which have a complex internal structure. The stability of the superhydrophobic surface coating was found to be acceptable when the coated materials were stored in dry conditions but under operating conditions where water was condensed onto the surfaces they degraded rapidly (within hours) due to corrosion. For this reason a second method of preparing superhydrophobic coatings by applying a layer of superhydropobic copper powder was developed. This powder has been extensively tested and is known to be stable against corrosion for periods of months to years. Imaging of the internal surfaces of the copper powder coated exchangers

showed that the coating method did not create a uniform thin layer of powder but instead there were areas where the coating was thicker which could block the air path and increase air-side pressure drop during the experiment. For comparison superhydrophilic coatings were also prepared.

To test the performance of the heat exchangers under normal operating conditions a model system which mimicked the operating conditions of an automobile air conditioning system was built. The inlet air temperature, relative humidity and velocity could be changed within the normal operating range i.e. around 33 ℃ and 1.0 m s^{-1} to 1.9 m s^{-1}. Initial tests showed there was a significant pressure drop in the system so dynamic dip tests were carried out. Importantly, these showed that the superhydrophobic coated heat exchangers held more water than the uncoated exchangers. This was found to be due to the design of the exchangers which were optimised for operation without a coating and had drainage holes to allow the water to escape from between the louvered fins. The superhydrophobic coating prevented the water from draining through these holes and therefore increased water retention. This effect could be removed by suspending the heat exchangers horizontally.

Further tests on the exchangers showed that they all retained condensation, which reduced the air flow through the system. Even under conditions where the superhydrophobic exchanger was freshly treated, had no corrosion and was used horizontally to eliminate water trapping the system still showed increasing air resistance with operating time due to build up of condensate. Since water droplets which were applied to the exchanger continued to roll freely off the surface the observation of droplets which were pinned to the surface was attributed to ‘flooding’ where the rate of condensation is so high

that droplets grow within the surface texture and are trapped before they can be shed.

The overall heat conductivities for all the heat exchangers were tested in both vertical and horizontal orientation. In the case of the superhydrophobic coated exchangers the UA was found to be either similar to or slightly higher than the uncoated systems. There were some indications that there was an effect due to some dropwise condensation but the effect was small. Of course increased heat transfer by dropwise condensation would have been excellent but not having a large improvement would not have been a significant problem if the coatings had performed as hoped and also reduced the amount of condensate on the fins, reducing the pressure drop. However, the effect of adding the coating was to increase the pressure drop, even in the absence of any condensate, and in operation it was found that the surfaces did not shed the condensed water in the same way that they shed liquid droplets placed onto the surface. The increased pressure drop meant that even if the UA was the same or slightly better than for the uncoated exchangers, the overall performance of the coated systems was actually worse. The exception was the superhydrophillic coatings which, in agreement with the literature gave similar UA values to the uncoated exchangers and have less water retention so may offer a small performance improvement.

4.2 Future Work

The system built in this research was designed to test if the superhydrophobic coatings developed here could give significant performance advantages that would ultimately be sufficient to justify the cost of applying them to commercial exchangers. The system used for the testing

was very simple but it was sufficient to allow the main conclusions about the performance of the coated exchangers to be determined. In the future if the exchanger performance can be improved then a more complex closed system should be constructed to allow them to be tested more rigorously. This will be a significant task since typical test systems of this type are typically designed to be built with fixed components and then operated under a range of conditions rather than being constantly modified with the exchangers being routinely changed.

Some of the problems encountered in this work, such as the degradation of the coatings would be problematic for real world applications at this stage but could be addressed with further work. Similarly, the design of the heat exchangers is clearly optimised for uncoated operation which actually makes them quite inappropriate for use with superhydrophobic coatings. Again this is an issue that could reasonably be addressed in future work.

On a more fundamental level, the main unknown arising from this work is the extent to which the problem of flooding can be addressed. It has been recognised as a limitation in the literature. However, preliminary work on planar substrates with electrolessly deposited coatings suggested that it was not a significant problem with coatings of this type so it will be useful to carry out much more detailed studies to understand the coating parameters that need to be achieved on the actual heat exchangers than will allow them to show this effect.

Reference

1. W. Barthlott and C. Neinhuis, *Planta*, 1997, **202**, 1-8.
2. P. Bertoldi and B. Atanasiu, *Electricity Consumption and Efficiency Trends in European Union* European Commission, Joint Research Centre, Institute for Energy Luxemburg, 2009.
3. I. Knight, *REHVA Journal*, 2012,**1**,17.
4. T. Young, *Philosophical Transactions of the Royal Society of London*, 1805, **95**, 65-87.
5. R. N. Wenzel, *Industrial & Engineering Chemistry*, 1936, **28**, 988-994.
6. A. B. D. Cassie and S. Baxter, *Transactions of the Faraday Society*, 1944, **40**, 546-551.
7. D. Polster and H. Graaf, *Applied Surface Science*, 2013, **265**, 88-93.
8. S. Wang and L. Jiang, *Advanced Materials*, 2007, **19**, 3423-3424.
9. P. Roah, N. J. Shirtcliffe and M. I. Newton, *Soft Matter*, 2008, **4**, 224-240.
10. D. Ebert and B. Bhushan, *Journal of Colloid and Interface Science*, 2012, **384**, 182-188.
11. G. S. Watson, B. W. Cribb and J. A. Watson, *ACS Nano*, 2010, **4**, 129-136.
12. M. Sun, G. S. Watson, Y. Zheng, J. A. Watson and A. Liang, *Journal of Experimental Biology*, 2009, **212**, 3148-3155.
13. T. Wagner, C. Neinhuis and W. Barthlott, *Acta Zoologica*, 1996, **77**, 213-225.
14. J. W. M. Bush, D. L. Hu and M. Prakash, in *Advances in Insect Physiology*, eds. J. Casas and S. J. Simpson, Academic Press, 2007, **34**, 117-192.
15. X. Zhang, J. Yan, J. Zhao, Y. Wang and Q. Pan, *AIP Advances*, 2014, **4**, 047118.
16. S. H. T. Nguyen, H. K. Webb, J. Hasan, M. J. Tobin, R. J. Crawford and E. P. Ivanova, *Colloids and Surfaces B: Biointerfaces*, 2013, **106**, 126-134.
17. H. J. Ensikat, P. Ditsche-Kuru, C. Neinhuis and W. Barthlott, *Beilstein Journal of Nanotechnology*, 2011, **2**, 152-161.
18. S. Yu and Z. Guo, *RSC Advances*, 2015, **5**, 107880-107888.
19. J. Liang, Y. Hu, Y. Wu and H. Chen, *Journal of Nanomaterials*, 2013, **2013**, 6
20. H. Liu, S. Szunerits, W. Xu and R. Boukherroub, *ACS Applied Materials & Interfaces*, 2009, **1**, 1150-1153.
21. P. Ragesh, V. Anand Ganesh, S. V. Nair and A. S. Nair, *Journal of Materials Chemistry A*, 2014, **2**, 14773-14797.

22. H. Zhang, L. Yin, X. Liu, R. Weng, Y. Wang and Z. Wu, *Applied Surface Science*, 2016, **380**, 178-184.
23. S. Lyu, D. C. Nguyen, D. Kim, W. Hwang and B. Yoon, *Applied Surface Science*, 2013, **286**, 206-211.
24. W. Zhang, X. Lu, Z. Xin and C. Zhou, *Nanoscale*, 2015, **7**, 19476-19483.
25. X. Fang, Z. Yu, X. Sun, X. Liu and F. Qin, *Frontiers of Chemical Engineering in China*, 2009, **3**, 97-101.
26. M. Paunovic, M. Schlesinger and D. D. Snyder, in *Modern Electroplating*, John Wiley & Sons, Inc., 2010, 1-32.
27. W. Xi, Z. Qiao, C. Zhu, A. Jia and M. Li, *Applied Surface Science*, 2009, **255**, 4836-4839.
28. M. H. Kwon, W. Y. Jee and C. N. Chu, *International Journal of Precision Engineering and Manufacturing*, 2015, **16**, 877-882.
29. B. Pijáková, M. Klíma, M. Alberti and V. Buršíková, *Materials Letters*, 2016, **184**, 243-247.
30. C. Wang, F. Tang, Q. Li, Y. Zhang and X. Wang, *Colloids and Surfaces A: Physicochemical and Engineering Aspects*, 2017, **514**, 236-242.
31. W. Wu, X. Wang, X. Liu and F. Zhou, *ACS Applied Materials & Interfaces*, 2009, **1**, 1656-1661.
32. H. Ogihara, J. Xie, J. Okagaki and T. Saji, *Langmuir*, 2012, **28**, 4605-4608.
33. Y. Y. Yan, N. Gao and W. Barthlott, *Advances in Colloid and Interface Science*, 2011, **169**, 80-105.
34. W. K. Cho and I. S. Choi, *Advanced Functional Materials*, 2008, **18**, 1089-1096.
35. J. Liu, W. Huang, Y. Xing, R. Li and J. Dai, *Journal of Sol-Gel Science and Technology*, 2011, **58**, 18-23.
36. M. Shi, J. Xi, H. Wang and X. Wu, *Journal of Adhesion Science and Technology*, 2008, **22**, 311-318.
37. W. Ma, H. Wu, Y. Higaki, H. Otsuka and A. Takahara, *Chemical Communications*, 2012, **48**, 6824-6826.
38. R. Taurino, E. Fabbri, M. Messori, F. Pilati, D. Pospiech and A. Synytska, *Journal of Colloid and Interface Science*, 2008, **325**, 149-156.
39. K. K. S. Lau, J. Bico, K. B. K. Teo, M. Chhowalla, G. A. J. Amaratunga, W. I. Milne, G. H. McKinley and K. K. Gleason, *Nano Letters*, 2003, **3**, 1701-1705.
40. S. Rezaei, I. Manoucheri, R. Moradian and B. Pourabbas, *Chemical Engineering Journal*, 2014, **252**, 11-16.
41. B. Qian and Z. Shen, *Langmuir*, 2005, **21**, 9007-9009.
42. J.-P. Lee, S. Choi and S. Park, *Langmuir*, 2011, **27**, 809-814.
43. Q. Wang, B. Zhang, M. Qu, J. Zhang and D. He, *Applied Surface Science*, 2008, **254**, 2009-2012.
44. I. A. Larmour, S. E. J. Bell and G. C. Saunders, *Angewandte Chemie*

International Edition, 2007, **46**, 1710-1712.
45. X. Xu, Z. Zhang and J. Yang, *Langmuir*, 2010, **26**, 3654-3658.
46. H. Ogihara, T. Katayama and T. Saji, *Journal of Materials Chemistry*, 2011, **21**, 14890-14896.
47. F. Tian, A. Hu, M. Li and D. Mao, *Applied Surface Science*, 2012, **258**, 3643-3646.
48. T. J. Wood, G. A. Hurst, W. C. E. Schofield, R. L. Thompson, G. Oswald, J. S. O. Evans, G. J. Sharples, C. Pearson, M. C. Petty and J. P. S. Badyal, *Journal of Materials Chemistry*, 2012, **22**, 3859-3867.
49. F. Muench, B. Juretzka, S. Narayan, A. Radetinac, S. Flege, S. Schaefer, R. W. Stark and W. Ensinger, *New Journal of Chemistry*, 2015, **39**, 6803-6812.
50. R. K. Shah, *Heat exchangers: Thermal-hydraulic fundamentals and designs*, Eds. Kakac, A. E. Bergles and F. Mayinger, New York, 1981, 9-46.
51. Q. Li, G. Flamant, X. Yuan, P. Neveu and L. Luo, *Renewable and Sustainable Energy Reviews*, 2011, **15**, 4855-4875.
52. A. Feneley, Troubleshooting your air conditioning (A/C) system, http://motorsportengineering.blogspot.co.uk/2009/02/troubleshooting-your-air-conditioning.html, 2017.
53. J. W. Rose, *Proceedings of the Institution of Mechanical Engineers, Part A: Journal of Power and Energy*, 2002, **216**, 115-128.
54. S. Kim and K. J. Kim, *Journal of Heat Transfer*, 2011, **133**, 081502-081502-081508.
55. B. Sikarwar, K. Muralidhar and S. Khandekar, *Interfacial Phenomena and Heat Transfer,* 2013, **1**, 339-356.
56. J. Su, M. Charmchi and H. Sun, *Scientific Reports,* 2016, **6**, 35132.
57. D. S. Kumar and R.Yuvaraj, presented in part at the Energy Efficient Technologies for Sustainability (ICEETS), Nagercoil, India, 10-12 April, 2013.
58. E. Schmidt, W. Schurig and W. Sellschopp, *Technische Mechanik und Thermodynamik*, 1930, **1**, 53-63.
59. E. J. Le Fevre and J. W. Rose, *3rd International Heat Transfer Conference,* Chicago, 1966.
60. H. W. Wen and R. M. Jer, *The Chemical Engineering Journal*, 1976, **12**, 225-231.
61. D. J. Preston, D. L. Mafra, N. Miljkovic, J. Kong and E. N. Wang, *Nano Letters*, 2015, **15**, 2902-2909.
62. J. B. Boreyko and C. H. Chen, *Physical Review Letters*, 2009, **103**, 184501.
63. K. Yanagisawa, M. Sakai, T. Isobe, S. Matsushita and A. Nakajima, *Applied Surface Science*, 2014, **315**, 212-221.
64. X. Chen, R. S. Patel, J. A. Weibel and S. V. Garimella, *Scientific Reports*, 2016, **6**, 18649.

65. C. Dietz, K. Rykaczewski, A. G. Fedorov and Y. Joshi, *Applied Physics Letters*, 2010, **97**, 033104.
66. H. Ji, A. Côté, D. Koshel, B. Terreault, G. Abel, P. Ducharme, G. Ross, S. Savoie and M. Gagné, *Thin Solid Films*, 2002, **405**, 104-108.
67. R. Sili, Y. Shengrong and Z. Yapu, *Acta Mechanica Sinica*, 2004, **20**, 159-164.
68. Z. Guo, F. Zhou, J. Hao and W. Liu, *Journal of the American Chemical Society*, 2005, **127**, 15670-15671.
69. D. K. Sarkar, M. Farzaneh and R. W. Paynter, *Materials Letters*, 2008, **62**, 1226-1229.
70. Q. Xu and J. Wang, *New Journal of Chemistry*, 2009, **33**, 734-738.
71. R. Menini and M. Farzaneh, *Surface and Coatings Technology*, 2009, **203**, 1941-1946.
72. N. R. Paluvai, H. Hafeez, D.-H. Han, H.-Y. Ryu, C.-S. Lee and J.-G. Park, *Journal of Adhesion Science and Technology*, 2017, **31**, 1061-1074.
73. E. B. Ratts and J. S. Brown, *International Journal of Thermal Sciences*, 2000, **39**, 592-604.
74. J. Gu, M. Kawaji, T. Smith-Pollard and J. Cotton*, ASME/JSME 2003 4th Joint Fluids Summer Engineering Conference*,2003.
75. G. H. Lee and J. Y. Yoo, *International Journal of Refrigeration*, 2000, **23**, 243-254.
76. J. M. S. Jabardo, W. G. Mamani and M. R. Ianella, *International Journal of Refrigeration*, 2002, **25**, 1157-1172.
77. S. Sannaye and M. Dehghandokht, *International Journal of Automotive Engineering*, 2012, **2**, 16.
78. M. E. Springer and K. A. Thole, *Experimental Thermal and Fluid Science*, 1999, **19**, 223-232.
79. Y. J. Chang, K. C. Hsu, Y. T. Lin and C. C. Wang, *International Journal of Heat and Mass Transfer*, 2000, **43**, 2237-2243.
80. M. H. Kim and C. W. Bullard, *International Journal of Refrigeration*, 2002, **25**, 390-400.
81. W. M. Yan and P. J. Sheen, *International Journal of Heat and Mass Transfer,* 2000,**43**,1651-1659.
82. G. J. Kim and A. M. Jacobi, *Condensate Accumulation Effects on the Air-Side Thermal Performance of Slit-Fin Surfaces*, Air Conditioning and Refrigeration Center,University of Illinois at Urbana-Champaign, 2000.
83. H. Osada, H. Aoki, T. Ohara and I. Kuroyanagi, *Heat Transfer—Asian Research*, 2001, **30**, 383-393.
84. J. Yin and A. M. Jacobi, University of Illinois, 2000.
85. G. Sir, Ö. Balioğlu and S. U. Onbaşıoğlu, *WIT Transactions on Engineering Sciences*, 2014, **83**, 9.
86. L. Liu, Ph.D. Thesis, University of Illinois at Urbana-Champaign, 2011.
87. L. Liu and A. M. Jacobi, *Journal of Heat Transfer*, 2009, **131**,

051802-051802-051809.
88. N. Miljkovic, R. Enright, Y. Nam, K. Lopez, N. Dou, J. Sack and E. N. Wang, *Nano Letters*, 2013, **13**, 179-187.
89. C. C. Wang and C. T. Chang, *International Journal of Heat and Mass Transfer*, 1998, **41**, 3109-3120.
90. K. Hong and R. L. Webb, *Journal of Heat Transfer*, 1999, **121**, 1018-1026.
91. C. C. Wang, W. S. Lee, W. J. Sheu and Y. J. Chang, *Applied Thermal Engineering*, 2002, **22**, 267-278.
92. S. Brennan, Ph.D.Thesis, Queen's University Belfast, 2011.
93. H. Abudayyeh, *Journal of Nanomaterials*, 2012, **2012**, 22 pages.
94. M. H. Kim and C. W. Bullard, *International Journal of Refrigeration*, 2002, **25**, 924-934.
95. S. Fotowat, Master Thesis, University of Windsor, 2012.
96. Vinayak S. Powar and M. M. Mirza, *Int.Journal Engineering Research and Applications*, 2013, **3**, 1409-1413.
97. T. A. Cowell, M. R. Heikal and A. Achaichia, *Experimental Thermal and Fluid Science*, 1995, **10**, 192-199.
98. MTA,*Instruction Manual for MTA Chiller*.
99. Y. Zhong, A. Joardar, Z. Gu, Y.-G. Park and A. M. Jacobi, *Experimental Thermal and Fluid Science*, 2005, **29**, 957-970.
100. L. Liu and A. M. Jacobi, *Experimental Thermal and Fluid Science*, 2008, **32**, 1512-1522.
101. I. A. Larmour, Ph.D.Thesis, Queen's University Belfast, 2008.
102. X. Yuan, Z. Tao, H. Li and Y. Tian, *Chinese Journal of Aeronautics*, 2016, **29**, 1575-1581.
103. C. M. Korte and A. M. Jacobi, *Condensation retention and shedding effects on Air-side heat exchanger performance Report* , Air conditioning and refrigeration center of University of Illinois, Urbana, 1997.
104. E. Ölçeroğlu and M. McCarthy, *ACS Applied Materials & Interfaces*, 2016, **8**, 5729-5736.

Appendix

Appendix A Steam Table

Table A.1 Properties of Saturated Steam.

Temperature T (℃)	Saturated Pressure P_s (bar)	Saturated Vapour Volume V_g (m3/kg)	Enthalpy(kJ/kg)			Entropy(kJ/kg • K)		
			Saturated liquid h_f	Evaporation	Saturated vapor h_g	Saturated liquid S_f	Evaporation	Saturated vapor S_g
0.01	0.006112	206.1	0	2500.8	2500.8	0	9.155	9.155
1	0.006566	192.6	4.2	2498.3	2502.5	0.015	9.113	9.128
2	0.007054	179.9	8.4	2495.9	2504.3	0.031	9.071	9.102
3	0.007575	168.2	12.6	2493.6	2506.2	0.046	8.978	9.024
4	0.008129	158.3	16.8	2491.3	2508.1	0.061	8.938	8.999
5	0.008719	147.1	21.0	2488.9	2509.9	0.076	8.898	8.974
6	0.009346	137.8	25.2	2486.6	2511.8	0.091	8.858	8.949
7	0.01001	129.1	29.4	2484.3	2513.7	0.106	8.818	8.924
8	0.01072	121.0	33.6	2481.9	2515.5	0.121	8.779	8.900
9	0.01147	113.4	37.8	2479.6	2517.4	0.136	8.74	8.876
10	0.01227	106.4	42.0	2477.2	2519.2	0.151	8.7	8.851

11	0.01312	99.90	46.2	2474.9	2521.1	0.166	8.662	8.828
12	0.01401	93.83	50.4	2472.5	2522.9	0.180	8.624	8.804
13	0.01497	88.17	54.6	2470.2	2524.8	0.195	8.585	8.780
14	0.01597	83.89	58.8	2467.8	2526.6	0.210	8.547	8.757
15	0.01704	77.97	62.9	2465.5	2528.4	0.224	8.51	8.734
16	0.01817	73.38	67.1	2463.1	2530.2	0.239	8.473	8.712
17	0.01936	69.09	71.3	2460.8	2532.1	0.253	8.436	8.689
18	0.02063	65.08	75.5	2458.4	2533.9	0.268	8.398	8.666
19	0.02196	61.34	79.7	2456	2535.7	0.282	8.362	8.644
20	0.02337	57.84	83.9	2453.7	2537.6	0.296	8.326	8.622
21	0.02486	54.56	88.0	2451.4	2539.4	0.310	8.29	8.600
22	0.02642	51.49	92.2	2449	2541.2	0.325	8.254	8.579
23	0.02808	48.62	96.4	2446.6	2543.0	0.339	8.218	8.557
24	0.02982	45.92	100.6	2444.2	2544.8	0.353	8.183	8.536
25	0.03166	43.40	104.8	2441.8	2546.6	0.367	8.148	8.515
26	0.03360	41.03	108.9	2439.5	2548.4	0.381	8.113	8.494
27	0.03564	38.81	113.1	2437.3	2550.4	0.395	8.078	8.473

28	0.03778	36.73	117.3	2434.8	2552.1	0.409	8.043	8.452
29	0.04004	34.77	121.5	2432.4	2553.9	0.425	7.987	8.412
30	0.04242	32.93	125.7	2430	2555.7	0.436	7.936	8.372
32	0.04754	29.57	134.0	2425.3	2559.3	0.464	7.868	8.332
34	0.05318	26.60	142.4	2420.5	2562.9	0.491	7.803	8.294
36	0.05940	23.97	150.7	2415.8	2566.5	0.518	7.738	8.256
38	0.06624	21.63	159.1	2411	2570.1	0.545	7.674	8.219
40	0.07375	19.55	167.5	2406.2	2573.7	0.572	7.61	8.182
42	0.08198	17.69	175.8	2401.4	2577.2	0.599	7.546	8.145
44	0.09100	16.03	184.2	2396.6	2580.8	0.625	7.486	8.111
46	0.1009	14.56	192.5	2398.9	2591.4	0.651	7.424	8.075
48	0.1116	13.23	200.9	2387	2587.9	0.678	7.313	7.991
50	0.1233	12.04	209.3	2382.1	2591.4	0.704	7.205	7.909
55	0.1574	9.578	230.2	2370.1	2600.3	0.768	7.062	7.830
60	0.1992	7.678	251.1	2357.9	2609.0	0.831	6.924	7.755
65	0.2501	6.201	272.0	2345.7	2617.7	0.893	6.788	7.681
70	0.3116	5.045	293.0	2333.3	2626.3	0.955	6.656	7.611

Appendix B Experiments Data and Results for Section 3.8.2

Table A.2 Heat Exchangers Mounted Vertically.

	Uncoated Heat Exchanger				Powder Coated Exchanger		Superhydrophilic Heat Exchanger				Zincated Exchanger	
	V_{in} = 1 m/s	V_{in} = 1.3 m/s	V_{in} = 1.5 m/s	V_{in} = 1.7 m/s	V_{in} = 1 m/s	V_{in} = 1.7 m/s	V_{in} = 1 m/s	V_{in} = 1.3 m/s	V_{in} = 1.5m/s	V_{in} = 1.7m/s	V_{in} = 1m/s	V_{in} = 1.7m/s
Ta1 (℃)	33.27	33.26	33.22	33.24	33.27	33.26	33.11	33.33	33.12	33.20	33.37	33.43
RH1 (%)	54.23	53.38	53.89	53.78	52.14	52.45	55.95	52.82	53.87	54.47	53.31	52.92
H1 （kg/kg）	0.018	0.017	0.017	0.017	0.017	0.017	0.018	0.017	0.017	0.018	0.017	0.017
Ta2 (℃)	8.05	7.41	8.13	8.67	5.79	6.38	7.53	6.24	7.16	7.70	7.12	6.59
RH2 (%)	75.46	83.12	74.47	85.26	68.50	72.03	70.57	72.12	71.46	80.66	71.53	74.57
H2 （kg/kg）	0.005	0.005	0.005	0.006	0.004	0.004	0.005	0.004	0.004	0.005	0.004	0.005
Tw1 (℃)	6.27	5.91	6.09	8.32	5.46	6.19	6.53	5.49	5.77	6.57	5.73	6.33
Tw2 (℃)	6.66	6.93	7.24	8.86	5.60	6.47	7.62	7.26	6.53	7.25	6.44	7.66
Ps_{inlet} (kPa)	5.1206	5.1206	5.0924	5.0924	5.1206	5.1206	5.0642	5.1206	5.0642	5.0924	5.1488	5.1488
Pw_{inlet} (kPa)	2.7769	2.7335	2.7445	2.7388	2.6696	2.6856	2.8334	2.7048	2.7282	2.7736	2.7448	2.7246
Ps_{outlet} (kPa)	1.0720	1.0294	1.0795	1.1245	0.92206	0.96116	1.0365	0.9479	1.0152	1.0507	1.0081	1.0436
Pw_{outlet} (kPa)	0.8089	0.8557	0.8040	0.9587	0.6316	0.6924	0.7315	0.6836	0.7254	0.8475	0.7211	0.7782
Density (kg/m^3)	1.1363347	1.136585	1.1366714	1.1366324	1.1368225	1.1367663	1.1366817	1.1364267	1.137123	1.136619	1.1361118	1.135987
Mass flow (kg/s)	0.009	0.012	0.014	0.015	0.009	0.015	0.009	0.012	0.014	0.015	0.009	0.015
LMTD	9.181	8.656	9.404	5.660	6.166	5.370	7.564	7.123	8.534	7.925	8.622	5.539
Qa (kJ)	0.582	0.744	0.864	0.924	0.614	1.022	0.609	0.790	0.892	0.982	0.601	1.007
UA (W/K)	63.401	85.913	91.864	163.257	99.583	190.286	80.504	110.927	104.530	123.879	69.660	181.879

Table A.3 Heat Exchangers Mounted Horizontally.

	Uncoated Heat Exchanger				Zincated Heat Exchanger				Powder Coated Exchanger	
	V_{in} = 1 m/s	V_{in} = 1.3 m/s	V_{in} = 1.6 m/s	V_{in} = 1.9 m/s	V_{in} = 1 m/s	V_{in} = 1.3 m/s	V_{in} = 1.6 m/s	V_{in} = 1.9 m/s	V_{in} = 1 m/s	V_{in} = 1.9 m/s
Ta1 (℃)	33.33	33.50	33.38	33.32	33.33	33.50	33.38	33.32	33.33	33.41
RH1 (%)	54.300	52.890	51.400	55.160	54.300	52.890	51.400	55.160	51.410	53.493
H1 (kg/kg）	0.018	0.017	0.017	0.018	0.018	0.017	0.017	0.018	0.017	0.017
Ta2 (℃)	8.21	6.95	6.74	7.80	8.21	6.95	6.74	7.80	7.09	6.50
RH2 (%)	77.023	72.985	71.537	80.666	77.023	72.985	71.537	80.666	65.243	59.757
H2 (kg/kg）	0.0052	0.0045	0.0043	0.0053	0.0052	0.0045	0.0043	0.0053	0.0041	0.0036
Tw1 (℃)	7.05	6.42	6.37	6.54	7.05	6.42	6.37	6.54	6.84	5.82
Tw2 (℃)	9.38	8.33	7.33	8.02	9.38	8.33	7.33	8.02	8.19	7.92
Ps_{inlet} (kPa)	5.1206	5.177	5.1488	5.1206	5.1206	5.177	5.1488	5.1206	5.1206	5.1488
Pw_{inlet} (kPa)	2.780	2.738	2.646	2.825	2.780	2.738	2.646	2.825	2.633	2.754
Ps_{outlet} (kPa)	1.087	1.001	0.98108	1.0578	1.087	1.001	0.98108	1.0578	1.0081	0.9678
Pw_{outlet} (kPa)	0.837	0.731	0.702	0.853	0.837	0.731	0.702	0.853	0.658	0.578
Density (kg/m^3)	1.136	1.136	1.137	1.136	1.136	1.136	1.137	1.136	1.137	1.136
Mass flow (kg/s)	0.009	0.012	0.015	0.017	0.009	0.012	0.015	0.017	0.009	0.017
LMTD	7.521	6.395	6.047	8.011	7.521	6.395	6.047	8.011	5.385	6.852
Qa (kJ)	0.577	0.780	0.944	1.113	0.577	0.780	0.944	1.113	0.591	1.202
UA (W/K)	76.693	122.043	156.087	138.900	76.693	122.043	156.087	138.900	109.828	175.453